

Double scaling limit of the prismatic tensor model

T. Krajewski¹, T. Muller ^{*2}, and A. Tanasa^{2,3}

¹Aix Marseille Univ, Université de Toulon, CNRS, CPT, Marseille, France, EU

²Univ. Bordeaux, LaBRI CNRS UMR 5800, Talence, France, EU

³DFT, H. Hulubei Nat. Inst. Phys. Nucl. Engineering, Magurele, Magurele, Romania, EU

April 25, 2023

Abstract

In S. Giombi, I. Klebanov, F. Popov, S. Prakash and G. Tarnopolsky, *Phys. Rev. D* 98 (2018) 10, 105005, a prismatic tensor model was introduced. We study here the diagrammatics and the double scaling limit of this model, using the intermediate field method. We explicitly exhibit the next-to-leading order Feynman graphs in the $1/N$ expansion. Using appropriate combinatorial tools, we further study the general term of the $1/N$ expansion and we compute the 2–point function in the double scaling limit. We find that the double scaling limit mechanism implemented here is similar to the one implemented for various quartic tensor models.

Contents

1	Introduction	2
2	Brief review on the double scaling limit	4
3	The prismatic model; intermediate field method	5
4	Leading order graphs in the large N limit	9
4.1	Leading order graphs in the tetrahedric representation	9
4.2	Leading order graphs in the prismatic representation	11
5	Generating functions of leading order graphs	11
5.1	Generating functions of melonic graphs	11
5.2	Generating function of LO graphs in the prismatic representation . .	14

*corresponding author

6	Diagrammatic Analysis	15
6.1	Dipoles and their generating functions	15
6.2	Chains and their generating functions	16
6.3	Scheme decomposition	22
7	Next-to-leading order graphs	26
7.1	Dipole-free 2 particle irreducible graphs	26
7.2	2PI graphs with dipoles	27
7.3	2 particle reducible NLO graphs	28
8	Double scaling limit of the 2-point function	29
9	Free energy in the double scaling limit	34
10	Concluding remarks	36

1 Introduction

Tensor models are zero-dimensional quantum field theoretical models where the fields are tensors of arbitrary rank (see the books [1] [2] or the review articles [3], [4], [5], [6] or [7]).

Introduced as a generalization in dimension three and higher of the celebrated random matrix models (see [8] and the reviews [9, 10]), tensor models are currently studied in the context of mathematical physics, combinatorics and various other domains of mathematics. Thus, rank d tensor models are naturally linked to d -dimensional random geometries, as the Feynman graphs present in their perturbative expansion are dual to random triangulations. Moreover, such models were proven by Witten [11] and then by Klebanov and Tarnopolsky [12] to be related to the holographic Sachdev-Ye-Kitaev model [13].

Initially proposed in the nineties (see, for example, [14]), tensor models lacked the implementation of the large N mechanism (N being in this context the size of the tensor). This changed in 2011, with the proposition of the so-called colored tensor model by Gurau [15], which he proved to have a well-defined large N expansion [16]. Shortly after, a less restricted model (from the point of view of the class of Feynman graphs allowed by the perturbative expansion), the multi-orientable model [17] was proposed and proven to have a well-defined large N expansion [18].

An $O(N)^3$ -invariant tensor model, was proposed in [19] (see also [20, 21] for various diagrammatic developments). We refer to this type of model as single field tetrahedric model, since one has only one tensor field in the action, and the interaction is tetrahedric (its index structure has the topology of a tetrahedron).

Let us also mention that the model proposed in [19] was later related by Klebanov and Tarnopolsky in [12] to the celebrated holographic SYK model.

The case of sextic interactions for this type of $O(N)^3$ invariant-tensor model was studied by Giombi et al. in [22]. This model was called prismatic since its large N limit is dominated by a positive-definite operator whose index structure has the topology of a prism. In this paper, we will study this prismatic model.

Let us recall that the large N expansion of tensor models is controlled, as usually in tensor models, by a parameter ω called the degree. The large N expansion is dominated by graphs of vanishing degree. In [23], it was proven that the leading

order (LO) graphs in the large N expansion of the prismatic model are not the usual melonic graphs one is used to from tensor model literature (see again the books [1] [2] or the review articles [3], [4], [5] or [7]). The role of the fundamental melon is played by a triple tadpole graph. Moreover, one now has two types of melonic insertions, one at the level of the propagator (as usually in tensor model literature), and another one at the level of the vertex, which is a new type of melonic move with respect to what it is known in the tensor model literature.

In this paper we give a different proof of the LO graph identification of [23]. Our proof relies on an extensive use of the intermediate field method, which expresses the prismatic model as a model with quartic tetrahedric interactions, but with two distinct tensor field (the initial tensor field and an intermediate field).

Moreover, the intermediate field method used in this papers allows us to identify the next-to-leading (NLO) graphs in the large N expansion.

The main result of this paper is then the implementation of the celebrated double scaling limit mechanism for the prismatic tensor model. Using a combinatorial scheme decomposition *a la* [24] allows to identify at any degree a sub-family of graphs, called dominant, whose amplitude is the most divergent when the coupling constant of the model goes to criticality. One then has, in this double scaling limit, contributions of Feynman graphs of any degree, as it was already noticed for the colored [25] model, the multi-orientable model [26] and the single field tetrahedric model [20].

Note that in this paper we work with the 2-point function, and not with the free energy when implementing the double scaling mechanism. This comes from the fact that, from a combinatorial point of view, it is easier to work with the 2-point function, which correspond to what combinatorists call a *rooted* graph (and which has no symmetries). This is a standard tool in combinatorics and it has already been exported in mathematical physics for the study of quartic tensor models (see again [20], [26] and [25]). However, the results obtained here for the 2-point function can be extended, leading to an analogous behaviour, for the free energy (or for $2k$ -point function, k here being arbitrary, see [26], where this was implemented for the multi-orientable tensor model).

Moreover, we prove that the 2-point function of the model is summable in the double scaling limit. This behaviour is different with respect to the matrix model case.

In this paper, our overall strategy is the following:

1. Apply the intermediate field method in order to reduce the sextic interaction of the prismatic model to the quartic, tetrahedric one. As mentioned above, by doing so, one now has two fields in the action, the original tensor field and the intermediate field (also a tensor field). We call this the tetrahedric representation of the model (by contrast to the "original" one, using the prismatic vertex, which we call the prismatic representation of the model).
2. Generalize the results known in the case of the single field tetrahedric model mentioned above to the two-field model obtained *via* the use of the intermediate field method.
3. When possible, deduce the results on the original prismatic model from the two field model above (thus somehow applying an "inverse" intermediate field method).

Let us mention that deducing some of the results on the original prismatic model from the two field model above does not appear to us to be direct, since some of the combinatorial tools used here are natural for quartic interactions but are not transposable in a direct way from the quartic model to the sextic model.

Note however that even though in [22] the prismatic model is studied in dimension $3 - \varepsilon$, the double scaling limit mechanism we implement in this paper is done for a 0-dimensional prismatic tensor model. It does not seem clear to us if our results can easily generalize to the dimension $3 - \varepsilon$ case.

For the sake of completeness, let us also mention that some sixth order tensor models (but not the prismatic model studied in this paper), as well as other types of tensor models, have also been studied in [27], where the authors have analysed the dominant regime and critical behaviour of their models.

The paper is structured in the following way. In the next section, we give a short review of the double scaling limit mechanism of matrix and quartic tensor models. In the third section, we recall the definition of the prismatic model and the use of the intermediate field method in this case. In the fourth section, we exhibit the LO graphs, in both the tetrahedric and the prismatic representations of the model. In the following section, we study the generating functions of the LO graphs, in both representations of the model. In the sixth section we introduce appropriate diagrammatic tools in order to study, from a combinatorial point of view, the general term of the large N expansion of this model. We use these tools in the following sections, where the NLO Feynman graphs are exhibited. In the eighth section we identify the dominant graphs and compute the 2-point function in the double scaling limit. In the ninth section we obtain, from the 2-point function in the double scaling limit, the free energy in the double scaling limit. We end the paper with a concluding section.

2 Brief review on the double scaling limit

In this section, we give a short review of the large N limit and the double scaling limit of matrix and quartic tensor models.

For both models, the quantities of interests, such as the partition function, can be expanded in terms of Feynman graphs and rearranged in powers of $\frac{1}{N}$. However, the nature of this expansion differs between the two models.

On the one hand, matrix models [28, 29] expand in ribbon graphs. This $\frac{1}{N}$ -expansion is controlled by the genus g of these Feynman ribbon graphs. The partition function of these models writes:

$$Z_M(\lambda) = \sum_{g=0} N^{2-2g} Z_g(\lambda) ,$$

where λ is the coupling constant of the interaction and $Z_g(\lambda)$ is the contribution of all the genus g graphs. In the large N limit, only $Z_0(\lambda)$ contributes - planar graphs are dominating the expansion.

On the other hand, rank D quartic tensor models expand in terms of $D + 1$ edge-colorable graphs and their $\frac{1}{N}$ expansion is controlled by Gurau's degree ω . The partition function of these models writes:

$$Z_T(\lambda) = \sum_{\omega} N^{3-\omega} Z_{\omega}(\lambda)$$

Unlike the genus g , the degree is not a topological invariant. Again, in the large N limit only the term $Z_0(\lambda)$ contributes, which corresponds to the so-called melonic graphs.

Let us now recall the double scaling limit mechanism for matrix and quartic tensor models. In the case of matrix models, one can prove that the coefficients at each order in the $\frac{1}{N}$ expansion behave as

$$Z_g(\lambda) \sim f_g(\lambda - \lambda_c)^{\frac{5}{2}(1-\gamma_{str})g/2} ,$$

with λ_c a critical value of the coupling constant where all the Z_g diverges and γ_{str} a critical exponent of the model. By defining a double scaling parameter κ as

$$\kappa^{-1} = N(\lambda - \lambda_c)^{2-\gamma_{str}/2} ,$$

one can rewrite the expansion as

$$Z_M(\lambda) = \sum_{g=0} \kappa^{2g-2} f_g .$$

The double scaling limit is then obtained by taking $N \rightarrow \infty$ and $\lambda \rightarrow \lambda_c$ while keeping κ constant. In this limit, Z_M has contribution of all graphs and not simply the planar ones however the series of $Z_M(\lambda)$ diverges.

For quartic tensor models, the double scaling limit mechanism is obtained in the following way. In the tensor model literature, the double scaling limit mechanism is to our knowledge only implemented for the 2-point or $2r$ -point functions (r being an integer). However, the free energy in the double scaling limit can be obtainable from the 2-point function, and this is explained in Section 3 below.

It was found for different models with tetrahedral interaction that the dominant graphs in the double scaling limit are bijection with rooted binary trees and that the 2-point function had an exact expression [25, 20, 26]. For example, in the case of the $O(N)^3$ -invariant model with tetrahedral interaction one finds

$$G_2^{DS} = M_c \left(1 + N^{11/12} \frac{\sqrt{3}\lambda_c^{1/2}}{(1+6\lambda_c^2)^{1/2}} \frac{1 - \sqrt{1-4\kappa}}{2\kappa} \right) ,$$

with κ the double scaling parameter proportional to

$$\kappa^{-1} \sim N^{\frac{1}{2}} \left(1 - \frac{\lambda^2}{\lambda_c^2} \right) .$$

3 The prismatic model; intermediate field method

In this section we recall from [22] the definition of the prismatic tensor model and the implementation of the intermediate field method for this model.

Let a random tensor $T_{i_1 i_2 i_3}$ with three indices ranging from 1 to $N \in \mathbb{N}^*$. The group $O(N)^3$ acts in the following way on the tensor field

$$T_{i_1 i_2 i_3} = O_{i_1 j_1}^{(1)} O_{i_2 j_2}^{(2)} O_{i_3 j_3}^{(3)} T_{j_1 j_2 j_3} , \tag{1}$$

where the $O^{(k)}$ are independent orthogonal matrices. The action of the model writes:

$$S_N = -\frac{1}{2} \sum_{i,j,k} T_{ijk} T_{ijk} + \frac{tN^{-\alpha}}{6} \sum_{a_1, a_2, a_3, b_1, b_2, b_3, c_1, c_2, c_3} T_{a_1 b_1 c_1} T_{a_1 b_2 c_2} T_{a_2 b_1 c_2} T_{a_3 b_3 c_1} T_{a_3 b_2 c_3} T_{a_2 b_3 c_3}, \quad (2)$$

$$S_N = -\frac{1}{2} \sum_{i,j,k} T_{ijk} T_{ijk} + \frac{tN^{-\alpha}}{6} I_p(T).$$

Where

$$I_p(T) = \sum_{a_1, a_2, a_3, b_1, b_2, b_3, c_1, c_2, c_3} T_{a_1 b_1 c_1} T_{a_1 b_2 c_2} T_{a_2 b_1 c_2} T_{a_3 b_3 c_1} T_{a_3 b_2 c_3} T_{a_2 b_3 c_3} \quad (3)$$

is the **prismatic tensor invariant** whose graphical representation is given in Fig 1. Let us note here that the prismatic interaction above is positively defined.

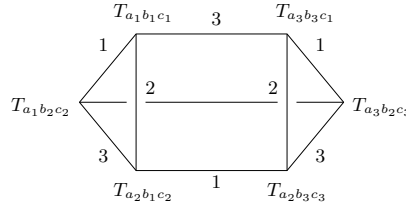


Figure 1: The prismatic interaction

The partition function is then given by

$$Z(t, N) = \int [dT] e^{-\frac{1}{2} \sum_{i,j,k} T_{ijk} T_{ijk} + \frac{tN^{-\alpha}}{6} I_p(T)}, \quad (4)$$

where $[dT]$ is the tensor measure

$$[dT] = \prod_{i,j,k=1}^N dT_{ijk}. \quad (5)$$

Using the intermediate field method, the sextic interaction above can be reduced to a quartic interaction [30]. Recall that

$$e^{\frac{tN^{-\alpha}}{6} I_p(T)} = \int \frac{[d\chi]}{(2\pi)^{N^3/2}} e^{-\frac{1}{2} \sum_{i,j,k=1}^N \chi_{ijk} \chi_{ijk}} e^{\sqrt{\frac{2tN^{-\alpha}}{6}} \sum_{a_1, a_2, b_1, b_2, c_1, c_2=1}^N T_{a_1 b_1 c_1} T_{a_1 b_2 c_2} T_{a_2 b_1 c_2} \chi_{a_2 b_2 c_1}}, \quad (6)$$

$$= \int \frac{[d\chi]}{(2\pi)^{N^3/2}} e^{-\frac{1}{2} \sum_{i,j,k=1}^N \chi_{ijk} \chi_{ijk} + \sqrt{\frac{2tN^{-\alpha}}{6}} \tilde{I}_t(T, \chi)},$$

where

$$\tilde{I}_t(T, \chi) = \sum_{a_1, a_2, b_1, b_2, c_1, c_2=1}^N T_{a_1 b_1 c_1} T_{a_1 b_2 c_2} T_{a_2 b_1 c_2} \chi_{a_2 b_2 c_1}. \quad (7)$$

The interaction obtained by using this intermediate field method is therefore a tetrahedron-type interaction coupling three T fields and one intermediate field χ . The graphical representation of this interaction is given in Fig 2.

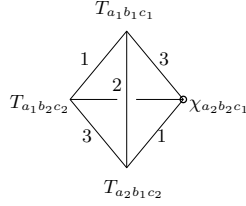


Figure 2: The tetrahedric interaction

The partition function can therefore be written as

$$\begin{aligned}
Z(t, N) &= \int [dT] \frac{[d\chi]}{(2\pi)^{N^3/2}} e^{-\frac{1}{2} \sum_{i,j,k=1}^N (T_{ijk} T_{ijk} + \chi_{ijk} \chi_{ijk}) + \sqrt{\frac{2tN-\alpha}{6}} \tilde{I}_t(T, \chi)}, \\
&= \int [dT] \frac{[d\chi]}{(2\pi)^{N^3/2}} e^{-\frac{1}{2} \sum_{i,j,k=1}^N (T_{ijk} T_{ijk} + \chi_{ijk} \chi_{ijk}) + \frac{\lambda' N^{-\alpha'}}{4} \tilde{I}_t(T, \chi)},
\end{aligned} \tag{8}$$

where we made a redefinition of the coupling constant $\frac{\lambda' N^{-\alpha'}}{4} = \sqrt{\frac{2tN-\alpha}{6}}$. The identification $2\alpha' = \alpha$ indicates that the scaling of a prismatic interaction needs to be twice the one of a tetrahedron. Recall that the single field tetrahedron interaction is known to be equal to $\frac{3}{2}$ [19]. One thus has, for the scaling parameter of the prismatic interaction:

$$\alpha = 3. \tag{9}$$

Expanding the interaction part of the action and using Wick's theorem, one can write the partition function as a formal power series in the coupling constant such that:

$$Z(t, N) = \sum_{n_p \in \mathbb{N}} \sum_{\mathcal{G} \in \mathbb{G}_{n_p}} A_{\mathcal{G}} t^{n_p}$$

Where the second sums runs over the set of vacuum 4-regular properly-edge-colored graphs such that the subgraph obtained by removing all the feynman edges¹ is a disjoint union of either n_p prismatic vertices, if no intermediate field was used, or $2n_p$ tetrahedric vertices, if one was introduced. The parameter $A_{\mathcal{G}}$ is the amplitudes of the graph \mathcal{G} . In the sequel, when working with prismatic vertices, it will be stated that the analysis is performed in the **prismatic representation**. When working with the intermediate field representation, hence with tetrahedron interactions, we will refer to it as the **tetrahedric representation**.

Using the intermediate field method described above, any prismatic vertex in a Feynman graph can be split into two tetrahedra vertices connected by an intermediate field propagator χ as in Figure 3, where the field χ is represented by a curly line.

Let us also notice that the tetrahedric representation can be linked to dimer models of the graphs present in the tetrahedric model. The dimer model is the study of the perfect matchings of a graph. Recall that a perfect matching of a graph is a configuration where all its vertices are paired with exactly one of their connected neighbours [31]. As each vertex possesses a single χ node, connecting two vertices with a χ propagator is equivalent to pairing them. Therefore, by considering

¹The "feynman" edges, obtained from Wick's theorem, are given the color 0 in the graphs.

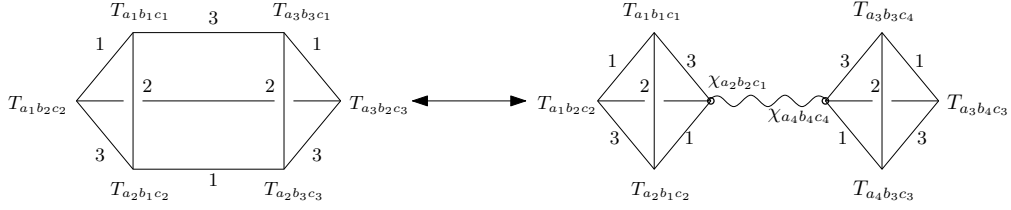


Figure 3: The intermediate field method for the prismatic tensor interaction.

the dimers of all the graphs in the tetrahedric model, one can derive all the graphs present in the tetrahedric representation of the prismatic model ². An example of the perfect pairing of a graph in the tetrahedric model and its equivalent in the tetrahedric representation is given in Figure 4.

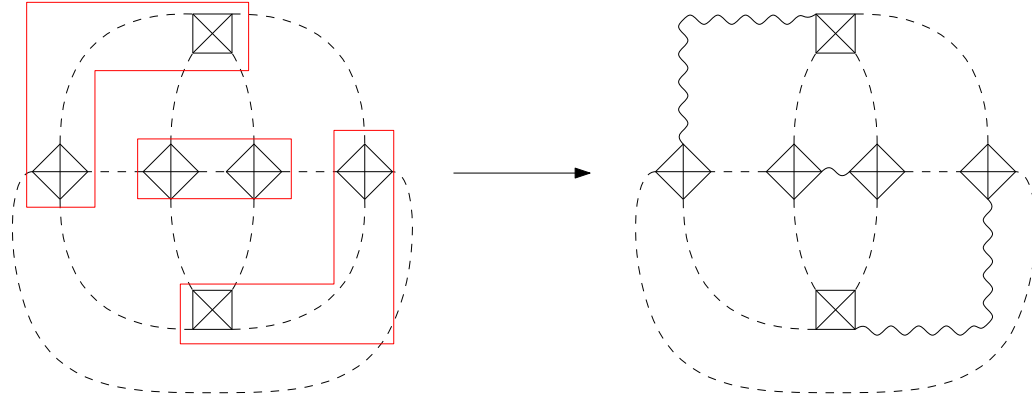


Figure 4: On the left, a graph in the tetrahedric model and one of its perfect pairings. On the right is the corresponding graph in the tetrahedric representation.

One can prove that the Feynman amplitude of a vacuum graph is proportional to

$$A_{\mathcal{G}} \propto N^{3-\omega(\mathcal{G})}, \quad (10)$$

where $\omega(\mathcal{G})$ is a parameter that we call the degree.

From each graph \mathcal{G} , one can define three jackets of color l by erasing the edges of the corresponding color in \mathcal{G} . These jackets can be treated as ribbon graphs with non orientable genus k_l (see [18]). Using Euler characteristic formula, one can find an expression for $\omega(\mathcal{G})$:

$$\omega(\mathcal{G}) = \sum_{l=1,2,3} \frac{k_l}{2} = 3 + 3n_p - f_{\mathcal{G}} = 3 + \frac{3}{2}n_t - f_{\mathcal{G}}. \quad (11)$$

In the equation above, $f_{\mathcal{G}}$ is the number of faces of the graph \mathcal{G} .

From the partition function one can define the free energy as

$$F(t, N) = -\frac{1}{N^3} \ln(Z).$$

²In a more general setting, replacing one of the fields in a single field interaction by an intermediate field is equivalent to consider the dimers of the graphs present in the original model.

and the 2–point function as

$$\langle T_{abc} T_{a'b'c'} \rangle = G_2(t) \delta_{aa'} \delta_{bb'} \delta_{cc'} ,$$

where $G_2(t) = \frac{1}{N^3} \langle \sum_{abc} T_{abc} T_{abc} \rangle$. Similarly to the partition function, $G_2(t)$ admits an expansion in terms of vacuum rooted graphs. Vacuum rooted graphs are vacuum graphs with a marked edge called the root. When studying the 2–point function in section 8, it will be understood that we work with rooted vacuum graphs.

To obtain the free energy $F(t, N)$ from the 2–point function, one can introduce a new parameter s such that $t = \tilde{t} s^3$ and a rescaled field \tilde{T} such that $T_{abc} = \frac{1}{\sqrt{s}} \tilde{T}_{abc}$. This introduces a parameter multiplying the quadratic part of the prismatic action. Denoting by a tilde the quantities with s introduced, the action rewrites

$$\tilde{S}_N = -\frac{1}{2} s^{-1} \sum_{i,j,k} \tilde{T}_{ijk} \tilde{T}_{ijk} + \frac{\tilde{t} N^{-3}}{6} I_p(\tilde{T})$$

and the free energy writes

$$\tilde{F}(s, \tilde{t}, N) = -\frac{1}{N^3} \ln \left(\int [d\tilde{T}] e^{-\frac{1}{2} s^{-1} \sum_{i,j,k} \tilde{T}_{ijk} \tilde{T}_{ijk} + \frac{\tilde{t} N^{-3}}{6} I_p(\tilde{T})} \right) .$$

The 2–point function of the rescaled field is also given by

$$\tilde{G}_2(\tilde{t}, s) = \sum_{a,b,c} \frac{1}{\tilde{Z}(s, \tilde{t}, N)} \int [d\tilde{T}] \frac{\tilde{T}_{abc} \tilde{T}_{abc}}{N^3} e^{-\frac{1}{2} s^{-1} \sum_{i,j,k} \tilde{T}_{ijk} \tilde{T}_{ijk} + \frac{\tilde{t} N^{-3}}{6} I_p(\tilde{T})} ,$$

$$\tilde{G}_2(\tilde{t}, s) = s G_2(\tilde{t} s^3) = \frac{2s^2}{N^3} \frac{1}{\tilde{Z}(s, \tilde{t}, N)} \frac{\partial \tilde{Z}(s, \tilde{t}, N)}{\partial s} = -2s^2 \frac{\partial \tilde{F}(s, \tilde{t}, N)}{\partial s} .$$

Integrating $-\frac{G_2(\tilde{t} s^3)}{2s}$, from $s = 0$ to $s = 1$ at fixed \tilde{t} gives then the original free energy since $\tilde{F}(s = 1, \tilde{t}, N) = F(t, N)$ and $F(s = 0, \tilde{t}, N) = 0$:

$$F(t, N) = - \int_0^1 \frac{ds}{2s} G_2(\tilde{t} s^3),$$

where we have used the fact that $\tilde{t} = t$ when $s = 1$.

4 Leading order graphs in the large N limit

In this section, we study the $\frac{1}{N}$ expansion of the prismatic model and we explicitly exhibit the dominant graphs, in both the tetrahedric and prismatic representation. Our study, as already mentioned in the Introduction, uses the intermediate field method.

4.1 Leading order graphs in the tetrahedric representation

Equation (11) above implies that the degree of the prismatic model is a non-negative integer. Hence, the LO Feynman graphs of the model are thus the ones satisfying the condition:

$$\omega(\mathcal{G}) = 0. \tag{12}$$

Let us first identify these graphs in the tetrahedric representation. As usual in the tensor model literature, we call these graphs melonic graphs. One can prove that they are built by starting from the vacuum elementary melon shown in Figure 5 and by recursively inserting one of the elementary 2-points melons on arbitrary edges. The insertions possible on the two types of edges are shown in Figure 6.

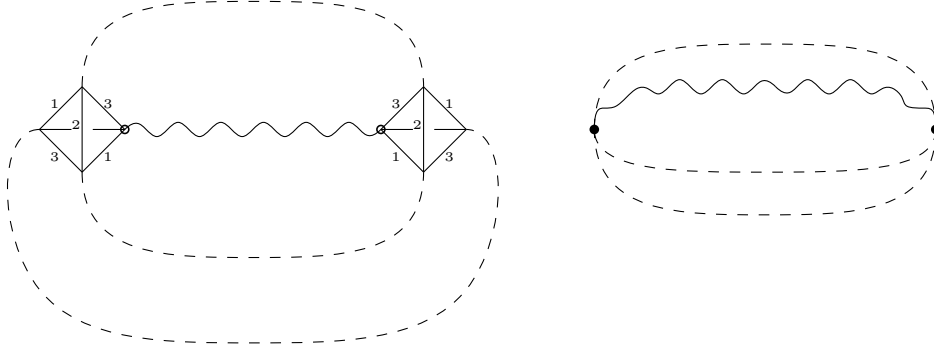


Figure 5: On the left, the vacuum elementary melon in the tetrahedric representation. On the right, a simplified graphical representation of the graph where the tetrahedric vertices are replaced by black dots.

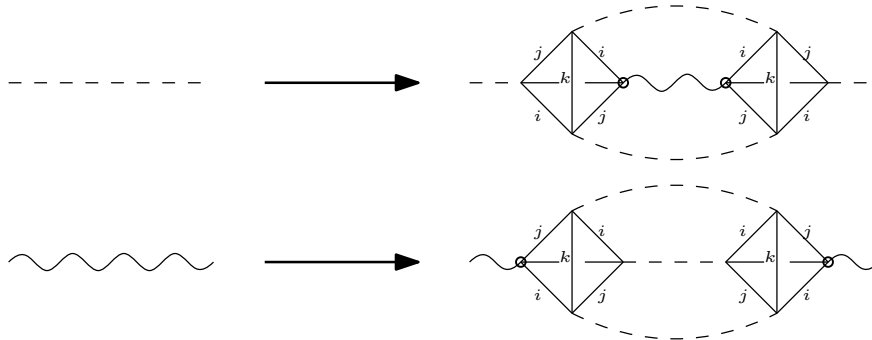


Figure 6: The melonic insertions on the two types of propagators.

Let us give in Fig. 7 an example of melonic graphs obtained *via* melonic insertions on a T propagator, on the LHS, and on a χ propagator on the RHS.

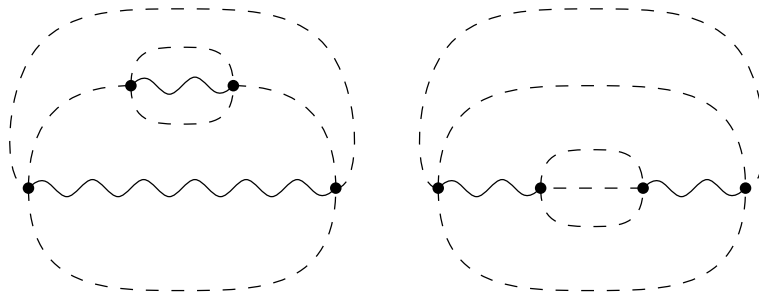


Figure 7: Example of melonic graphs.

4.2 Leading order graphs in the prismatic representation

In the prismatic representation, the elementary melon of the tetrahedric representation becomes a triple tadpole (see Figure 8 for its various graphical representations). We refer to this triple tadpole as the *elementary triple tadpole*.

Let us now explain what the two melonic insertions in the tetrahedric representation become in this prismatic representation. The insertion on a T propagator is equivalent to the insertion of a 2–point double tadpole (which is obtained by "cutting" an edge of the elementary triple tadpole). The insertion on a χ propagator is equivalent to an insertion at the level of a prismatic vertex. One needs to "split" a prismatic vertex into two prismatic vertices which are linked by T propagators (see Figure 9).

Let us give in Figure 10 some examples of LO graphs in the prismatic representation. The first graph is the elementary triple tadpole. The second graph is obtained by a vertex splitting of the elementary triple tadpole vertex. The third graph is obtained by inserting a 2–point double tadpole on one of the edges of the first graph (the elementary triple tadpole) and so on.

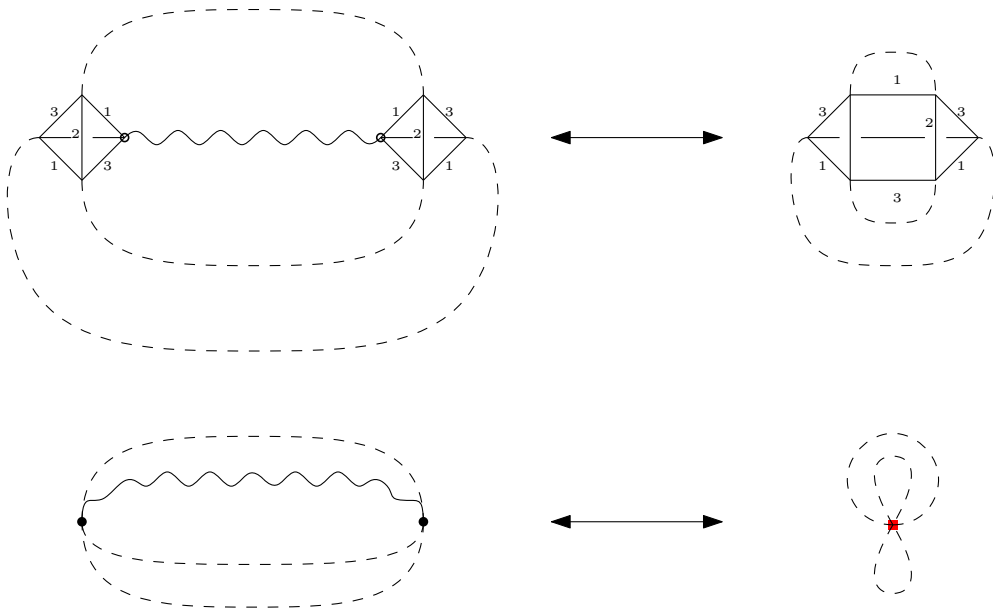


Figure 8: On the left, the elementary vacuum melon in the two graphical representations. On the right, their prismatic equivalent. On the bottom right, the prismatic vertex is represented by a red square.

5 Generating functions of leading order graphs

5.1 Generating functions of melonic graphs

In this subsection we analyse the generating functions of melonic graphs in the tetrahedric representation, find its singularities and the behaviour of this generating function close to the singularity.

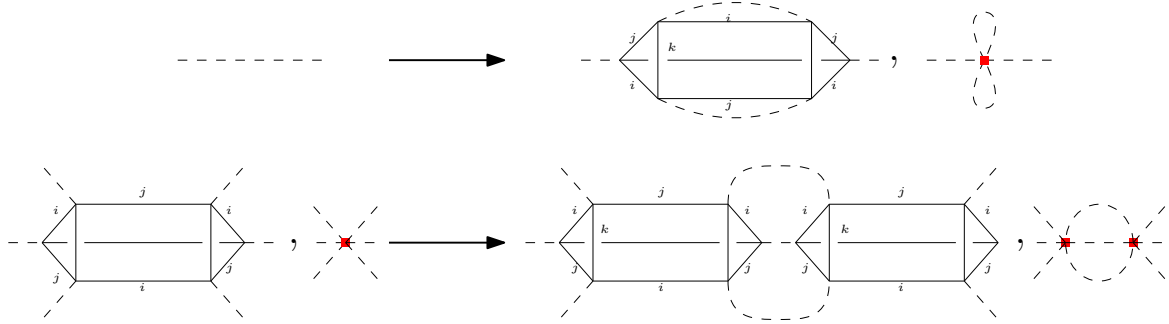


Figure 9: The prismatic equivalent of the two melonic insertions.

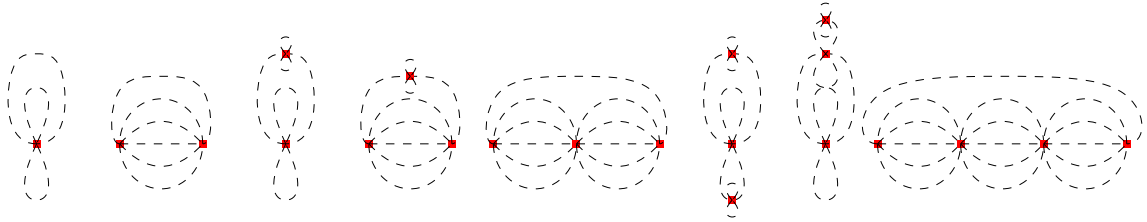


Figure 10: Examples of the LO graph in the prismatic representation.

As there are two types of 2–point functions (associated with the two propagators), we denote by $M_T(t)$ and $M_\chi(t)$ the generating functions of the two sets of corresponding melon graphs. This is given in Figure 11.

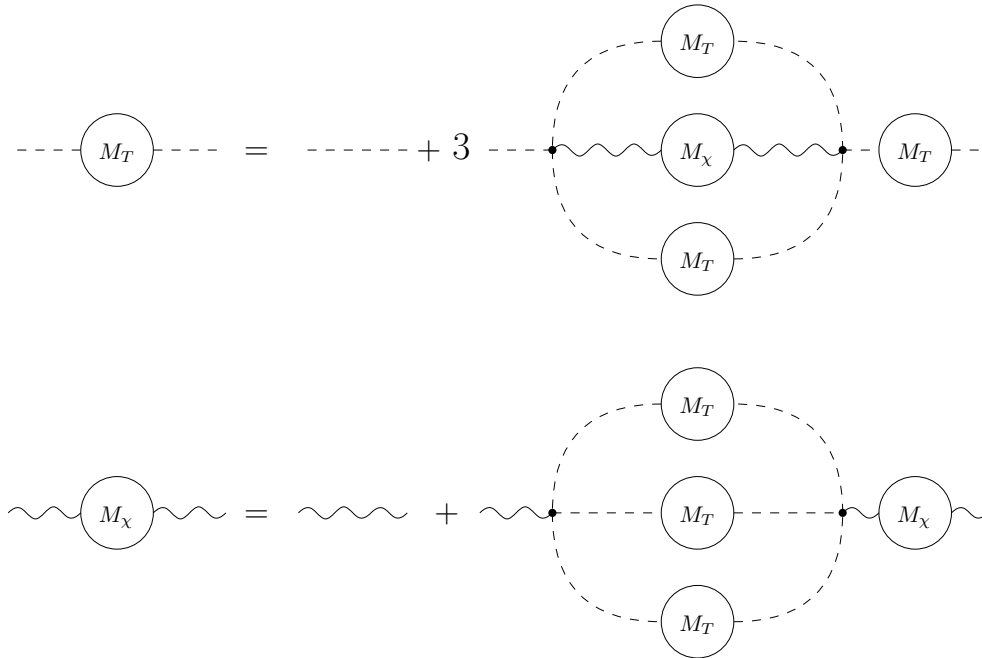


Figure 11: LO 2–point functions in the tetrahedric representation.

One has

$$\begin{aligned}
 M_T(t) &= 1 + 3tM_T^3(t)M_\chi(t), \\
 M_\chi(t) &= 1 + tM_T^3(t)M_\chi(t),
 \end{aligned}
 \tag{13}$$

where the factor 3 in the first equation above counts the three different choices of placing a χ propagator connecting the two vertices of the melonic graph. Substituting $M_\chi(t)$ in the first equation gives

$$1 + t(M_T^4(t) + 2M_T^3(t)) - M_T(t) = 0. \quad (14)$$

Finding the general solution of such equation is an involved task. However, one can derive its singularities, *i. e.* the points where the solution stops being analytic.

One can consider the more general problem given by

$$F(M_T, t) = 0, \quad (15)$$

where one needs to find $M_T(t)$. Using the implicit function theorem [32], one can write

$$\frac{dM_T(t)}{dt} = -\frac{\partial F/\partial t}{\partial F/\partial M_T}. \quad (16)$$

This implies that $M_T(t)$ ceases to be analytic when $\frac{\partial F}{\partial M_T} = 0$ as its derivative blows up.

In the case of the melons, one has $F(M_T, t) = 1 + t(M_T(t)^4 + 2M_T(t)^3) - M_T(t)$. One then has the following system of equations (we denote $M_T(t_c)$ by $M_{T,c}$):

$$\begin{aligned} M_{T,c} &= 1 + t_c(M_{T,c}^4 + 2M_{T,c}^3), \\ 1 &= t_c(4M_{T,c}^3 + 6M_{T,c}^2). \end{aligned} \quad (17)$$

The second equation implies $t_c = \frac{1}{4M_{T,c}^3 + 6M_{T,c}^2}$, which can be substituted in the first one to give

$$M_{T,c} = 1 + \frac{M_{T,c}^4 + 2M_{T,c}^3}{4M_{T,c}^3 + 6M_{T,c}^2}. \quad (18)$$

After some algebra, one finds $M_{T,c}^2 = 2$. The singularities are then the points for which $M_T = \pm\sqrt{2}$ at $t_c = \frac{1}{12 \pm 8\sqrt{2}}$. Recall that Pringsheim's theorem (see for example [32]) implies that the singularity closest to $t = 0$ defines the radius of convergence of the series expansion of $M_T(t)$ around the origin. This point is the dominant singularity. As $\frac{1}{12+8\sqrt{2}} < \frac{1}{12-8\sqrt{2}}$, one has

$$t_c = \frac{1}{12 + 8\sqrt{2}} \text{ and } M_T(t_c) = \sqrt{2}, \quad (19)$$

at the dominant singularity.

Let us now find the behavior of the function $M_T(t)$ near this dominant singularity. In order to do this, one needs to Taylor expand the function $F(M_T, t)$ near a critical point.

Assuming that $\frac{\partial^2 F}{\partial M_T^2} \neq 0$,

and using the conditions $F(M_T, t) = 0$, $\frac{\partial F}{\partial M_T}|_{t_c} = 0$ and since $\frac{\partial F}{\partial t^2} = 0$, one has:

$$\begin{aligned} \frac{\partial F}{\partial t}|_{t_c}(t_c - t) + \frac{\partial^2 F}{\partial t \partial M_T}|_{t_c}(t_c - t)(M_T(t) - M_{T,c}) + O(|t_c - t|^2) \\ = \frac{\partial^2 F}{\partial M_T^2}|_{t_c} \frac{1}{2}(M_T(t) - M_{T,c})^2. \end{aligned} \quad (20)$$

In the limit $t \rightarrow t_c$ (keeping only the LO term in the expansion), one has:

$$M_T(t) \stackrel{t \rightarrow t_c}{\sim} M_{T,c} \pm \sqrt{2 \frac{\partial F / \partial t|_{t_c}}{\partial^2 F / \partial M_T^2|_{t_c}}} \sqrt{t_c - t}. \quad (21)$$

Since $M_T(t)$ is the generating function of melonic graphs, this implies that $M_T(t)$ is an increasing function in t and this further implies that one needs to choose, amongst the two solutions (21), the solution with a negative sign.

Thus, the function $M_T(t)$ behaves, near the dominant singularity, as

$$\begin{aligned} M_T(t) &\stackrel{t \rightarrow t_c}{\sim} M_{T,c} - \sqrt{\frac{M_{T,c}^4 + 2M_{T,c}^3}{6(M_{T,c}^2 + M_{T,c})}} \sqrt{1 - t/t_c}, \\ M_T(t) &\stackrel{t \rightarrow t_c}{\sim} M_{T,c} - K \sqrt{1 - t/t_c}. \end{aligned} \quad (22)$$

Inserting the explicit expressions (19) of t_c and $M_{T,c}$, this behavior writes as

$$M_T(t) \stackrel{t \rightarrow t_c}{\sim} \sqrt{2} - \sqrt{\frac{\sqrt{2}}{3} \left(1 - \frac{t}{12 + 8\sqrt{2}}\right)}. \quad (23)$$

5.2 Generating function of LO graphs in the prismatic representation

In this subsection, we analyze the generating function of LO graphs in the prismatic representation and we give an enumerative combinatorics result for the number of such LO graph at an arbitrary order in perturbation theory.

Let us denote by P the generating function of the 2–point LO graphs. This expands as $P = \sum_n a_n t^n$. The coefficients a_n thus give us the number of LO graphs at a given order n in perturbation theory. In order to compute these coefficients, a closed equation for P needs to be found. This equation can be obtained in a diagrammatic way.

Recall that we found two distinct insertions (one at the level of the propagator and one at the level of the prismatic vertex) which generate all the LO graphs in the prismatic representation. This translates in the diagrammatic equation represented in Fig. 12, for the 2–point and 6–point function.

One has

$$\begin{aligned} P &= 1 + 3P^3\Gamma, \\ \Gamma &= t + tP^3\Gamma. \end{aligned} \quad (24)$$

This leads to

$$P - 1 = t(P^4 + 2P^3). \quad (25)$$

Changing variable to $y = P - 1$ gives

$$y = t((y + 1)^4 + 2(y + 1)^3) = tf(y). \quad (26)$$

Using Lagrange inversion theorem (see again the book [32]), the coefficient a_n can be computed in the following way. Suppose that $f(x)$ expands as $f(x) = \sum_{k \geq 0} f_k x^k$ and $f_0 \neq 0$. Then the equation $y = tf(y)$ admits a unique solution of the form $y(t) = \sum_{n \geq 1} y_n t^n$ with $y_n = \frac{1}{n} [x^{n-1}] f(x)^n$, where the notation $[x^m]g(x)$ denotes the order m coefficient of $g(x)$.

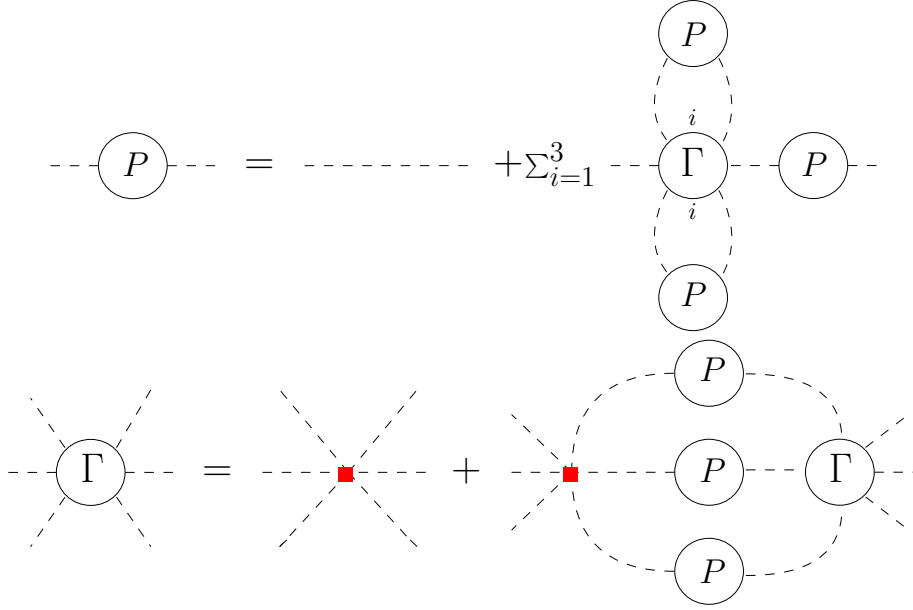


Figure 12: Graphical representation of the equations of the generating function P .

Recall that, in the case considered here, $f(y) = (y + 1)^4 + 2(y + 1)^3 = (y + 1)^3(y + 3)$. This implies that $y_n = \frac{1}{n}[x^{n-1}]((x + 1)^{3n}(x + 3)^n)$. Using the binomial expansion, one can identify the coefficients as

$$y_n = \frac{1}{n} \sum_{k \geq 0}^{n-1} \frac{3n!}{k!(3n-k)!} \frac{n!}{(n-k-1)!(k+1)!} 3^{k+1}. \quad (27)$$

Since $y = P - 1$, one thus has

$$P = 1 + \sum_{n \geq 1} \sum_{k \geq 0}^{n-1} \frac{3n!}{k!(3n-k)!} \frac{n!}{(n-k-1)!(k+1)!} 3^{k+1} t^n, \quad (28)$$

which finally leads to the identification of the number of LO graphs in the prismatic representation to be: $a_0 = 1$ and $a_n = y_n$, for any $n \in \mathbb{N}$.

6 Diagrammatic Analysis

In this section we introduce the diagrammatic tools needed to implement the double scaling limit of the model.

6.1 Dipoles and their generating functions

The notion of dipole was already introduced for the colored tensor model in [16], then for the MO tensor model in [33] and also for the $O(N)^3$ -invariant quartic model in [20]. In this subsection, we define a diagrammatic notion of dipole subgraph for the model studied here, in the tetrahedric representation.

A **dipole** of color i is a subgraph formed by two tetrahedric vertices connected by two parallel edges such that the subgraph has a face of length two and of color i .

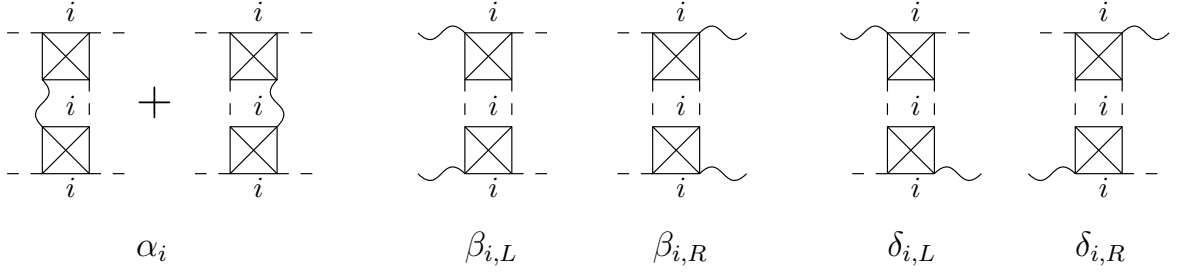


Figure 13: The five types of dipoles.

For each given color i , there are five different types of dipoles. We call these types of dipoles types α , β_L , β_R , δ_L and δ_R , see Fig. 13.

To simplify the graphical representation, the dipoles can be replaced by the dipole-vertices shown in Figure 14.



Figure 14: The five types of dipole-vertices.

Let us now exhibit the generating functions for the dipoles. One needs to insert the generating functions of melons on each edge and its square root on its half edges. This way of counting the melonic insertions on the edges allows us to avoid counting twice the melons when there are two adjacent dipoles.

Thus, the generating functions of the five types of dipoles write:

$$\begin{aligned}
 D_\alpha &= 2tM_T(t)^3M_\chi = \frac{2}{3}(M_T(t) - 1), \\
 D_{\beta_L} &= D_{\beta_R} = D_\beta = tM_T(t)^3M_\chi(t) = \frac{1}{3}(M_T(t) - 1) \\
 D_{\delta_L} &= D_{\delta_R} = D_\delta = tM_T(t)^3M_\chi(t) = \frac{1}{3}(M_T(t) - 1).
 \end{aligned} \tag{29}$$

Note that the generating function of a dipole does not depend on the color. Notice also that the generating functions of the dipoles of type β_L and β_R as well as the generating functions of the dipoles of type δ_L and δ_R are the same. In the following, we will differentiate the generating function of these dipoles when writing the structure of the chains (in Section 6.2). However, when writing the contribution of the dominant graphs to the 2–point function (in Section 8), we will simply denote them by D_β and D_δ . This allows us to clarify the structure of the chains while keeping a compact expression for the contribution of the dominant graphs.

From the expression of the different generating functions above, one can find that the critical points of the dipole generating functions are identical to the ones of the generating functions of the melon graphs.

6.2 Chains and their generating functions

Chains are defined in an analogous way as in [20] [33] to be the 4–point graphs obtained by connecting at least two dipoles and by matching one side of a dipole to the corresponding side of the next dipole in the chain.

A chain is said to be of length ℓ if it contains ℓ dipoles. Each chain of length ℓ contains subchains of length $2 \leq \ell' \leq \ell$. A chain is therefore said to be maximal if it cannot be included in a longer chain of the graph.

Note that changing the length of a chain doesn't change the degree of a graph. This can be proven by induction on the length of the chain, by inserting a dipole in a chain of length k , and by counting carefully the number of faces and vertices.

Using the previous five types of dipoles, there are eight different possibilities for the external edges of a chain. We thus have eight types of chains. If all the dipoles of a given chain are of color i , the respective chain is said to be an *unbroken* chain of color i . If the dipoles of the chain do not have the same color, we say that the respective chain is *broken*.

Similar to the case of dipoles, in order to simplify the graphics, we represent unbroken chains of a given type and color i by a chain-vertex C , while broken chains are represented by chain-vertices B . The different types of unbroken chain-vertices are shown in Figure 15.

Furthermore, we classify the chains into two families:

- Family A , if the external legs are the same on each side of the chain.
- Family B , if the external legs are different on each side of the chain.

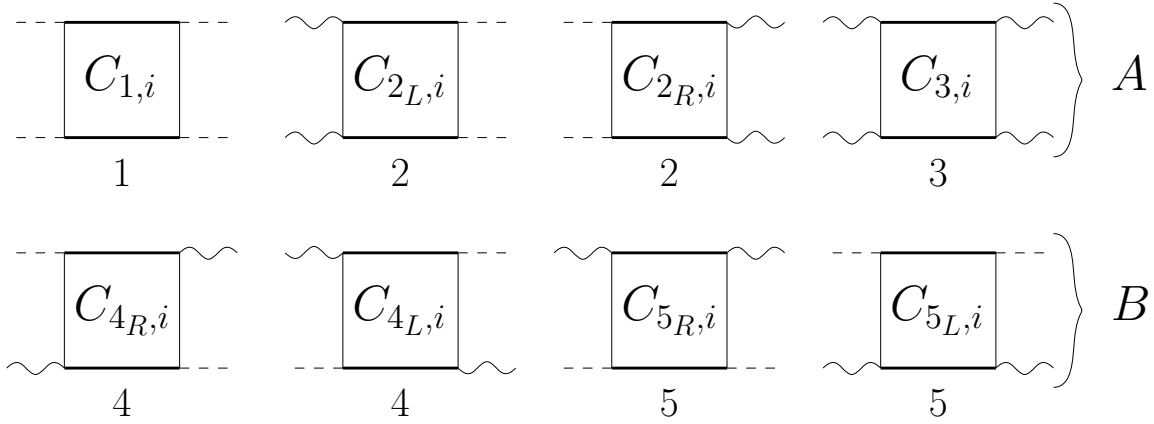


Figure 15: All the different types of broken chain-vertices.

Let us now have a closer look at the dipole structure and the generating functions of each of these chains:

Family A: The building block of the chains in the family A are the dipoles of type α , β_L and β_R . If a dipole of type β_R doesn't end a chain, it must be followed by a dipole of type β_L .

All the possibilities of gluing up dipoles are given in Figure 16. The other types of chains of the family A follow directly from the type 1 chain as shown in Figure 17.

$$\begin{aligned}
\boxed{C_{1,i}} &= \boxed{D_{\alpha,i}} \sum_{k \geq 1} \left(\boxed{D_{\beta_R,i}} \boxed{D_{\beta_L,i}} + \boxed{D_{\alpha,i}} \right)^k \\
+ \boxed{D_{\beta_R,i}} \boxed{D_{\beta_L,i}} \sum_{k \geq 0} &\left(\boxed{D_{\beta_R,i}} \boxed{D_{\beta_L,i}} + \boxed{D_{\alpha,i}} \right)^k
\end{aligned}$$

Figure 16: The structure of the chains of type 1.

$$\begin{aligned}
\boxed{C_{2L,i}} &= \boxed{D_{\beta_L,i}} \left(\boxed{C_{1,i}} + \boxed{D_{\alpha,i}} \right) \\
\boxed{C_{2R,i}} &= \left(\boxed{C_{1,i}} + \boxed{D_{\alpha,i}} \right) \boxed{D_{\beta_R,i}} \\
\boxed{C_{3,i}} &= \boxed{D_{\beta_L,i}} \left(\boxed{C_{1,i}} + \boxed{D_{\alpha,i}} \right) \\
&\quad + \boxed{D_{\beta_R,i}} + \boxed{D_{\beta_L,i}} \boxed{D_{\beta_R,i}}
\end{aligned}$$

Figure 17: The structure of the chains of type 2, 3.

The generating functions are then derived as following:

$$\begin{aligned}
C_1 &= D_\alpha \sum_{k \geq 1} (D_{\beta_R} D_{\beta_L} + D_\alpha)^k + D_{\beta_R} D_{\beta_L} \sum_{k \geq 0} (D_{\beta_R} D_{\beta_L} + D_\alpha)^k, \\
&= (D_\alpha + D_{\beta_R} D_{\beta_L}) \sum_{k \geq 0} (D_{\beta_R} D_{\beta_L} + D_\alpha)^k - D_\alpha, \\
&= \frac{D_\alpha + D_{\beta_R} D_{\beta_L}}{1 - (D_\alpha + D_{\beta_R} D_{\beta_L})} - D_\alpha,
\end{aligned} \tag{30}$$

and

$$\begin{aligned}
C_{2L} &= D_{\beta_L} (C_1 + D_\alpha) = D_{\beta_L} \frac{D_\alpha + D_{\beta_R} D_{\beta_L}}{1 - (D_\alpha + D_{\beta_R} D_{\beta_L})}, \\
C_{2R} &= D_{\beta_R} (C_1 + D_\alpha) = D_{\beta_R} \frac{D_\alpha + D_{\beta_R} D_{\beta_L}}{1 - (D_\alpha + D_{\beta_R} D_{\beta_L})}, \\
C_3 &= D_{\beta_L} (1 + C_1 + D_\alpha) D_{\beta_R} = \frac{D_{\beta_L} D_{\beta_R}}{1 - (D_\alpha + D_{\beta_R} D_{\beta_L})}.
\end{aligned} \tag{31}$$

The generating functions of the broken chains of type 1 can be derived from the expressions of the generating functions above by noticing that every chain of type 1 that is not of a given color must be broken. When building chains, there are three possible colors of dipoles to insert. Multiplying each generating functions of

dipoles by a factor three, and subtracting the chains of color i , gives the generating functions of the broken chains B_1 . This writes as:

$$B_1 = \frac{3D_\alpha + 9D_{\beta_L}D_{\beta_R}}{1 - (3D_\alpha + 9D_{\beta_L}D_{\beta_R})} - 3D_\alpha - \sum_{i=1,2,3} C_{1,i}. \quad (32)$$

The expressions of the remaining types of broken chains follow then from Figure 18 and write:

$$\begin{aligned} B_{2_L} &= 6D_{\beta_L}(C_1 + D_\alpha) + 3D_{\beta_L}B_1, \\ B_{2_R} &= 6(C_1 + D_\alpha)D_{\beta_R} + 3B_1D_{\beta_R}, \\ B_3 &= 24D_{\beta_L}(C_1 + D_\alpha)D_{\beta_R} + 6D_{\beta_L}D_{\beta_R} + 9D_{\beta_L}B_1D_{\beta_R}. \end{aligned} \quad (33)$$

$$\begin{aligned} \boxed{B_{2_L}} &= \sum_{i \neq j}^3 \boxed{D_{\beta_L,i}} \left(\boxed{C_{1,j}} + \boxed{D_{\alpha,j}} \right) \\ &\quad + \sum_{i=1}^3 \boxed{D_{\beta_L,i}} \boxed{B_1} \\ \boxed{B_{2_R}} &= \sum_{i \neq j}^3 \left(\boxed{C_{1,j}} + \boxed{D_{\alpha,j}} \right) \boxed{D_{\beta_R,i}} \\ &\quad + \sum_{i=1}^3 \boxed{B_1} \boxed{D_{\beta_R,i}} \\ \boxed{B_3} &= \sum_{\substack{i \neq j \text{ or } k \neq i \\ \text{or } k \neq j}}^3 \boxed{D_{\beta_L,i}} \left(\boxed{C_{1,j}} + \boxed{D_{\alpha,j}} \right) \\ &\quad + \boxed{D_{\beta_R,k}} + \sum_{i \neq j}^3 \boxed{D_{\beta_L,i}} \boxed{D_{\beta_R,j}} \\ &\quad + \sum_{i,j}^3 \boxed{D_{\beta_L,i}} \boxed{B_1} \boxed{D_{\beta_R,j}} \end{aligned}$$

Figure 18: The structure of the broken chains of family A.

After summing over the three colors in the last term of equation (32), and after some further algebra, one gets:

$$\begin{aligned} B_1 &= \frac{6D_{\beta_L}D_{\beta_R} + 18(D_{\beta_L}D_{\beta_R})^2 + 6D_\alpha^2 + 24D_\alpha D_{\beta_L}D_{\beta_R}}{(1 - (3D_\alpha + 9D_{\beta_L}D_{\beta_R}))(1 - (D_\alpha + D_{\beta_L}D_{\beta_R}))}, \\ B_{2_L} &= D_{\beta_L} \frac{24D_{\beta_L}D_{\beta_R} + 6D_\alpha}{(1 - (3D_\alpha + 9D_{\beta_L}D_{\beta_R}))(1 - (D_\alpha + D_{\beta_L}D_{\beta_R}))}, \\ B_{2_R} &= D_{\beta_R} \frac{24D_{\beta_L}D_{\beta_R} + 6D_\alpha}{(1 - (3D_\alpha + 9D_{\beta_L}D_{\beta_R}))(1 - (D_\alpha + D_{\beta_L}D_{\beta_R}))}, \\ B_3 &= \frac{3D_{\beta_L}D_{\beta_R}(2 + 6D_{\beta_L}D_{\beta_R})}{(1 - (3D_\alpha + 9D_{\beta_L}D_{\beta_R}))(1 - (D_\alpha + D_{\beta_L}D_{\beta_R}))}. \end{aligned} \quad (34)$$

Family B: As above, the structure of the chains in family B is derived from their building blocks that are dipoles of type δ_L and δ_R . If a dipole of type δ_L or resp. δ_R doesn't end a chain, it must be followed by a dipole of type δ_R or resp. δ_L . All the possibilities for type 5 chains are then given in Figure 19.

$$\begin{aligned}
C_{5R,i} &= D_{\delta_L,i} D_{\delta_R,i} \sum_{k \geq 0} \left(D_{\delta_L,i} D_{\delta_R,i} \right)^k \\
C_{5L,i} &= D_{\delta_R,i} D_{\delta_L,i} \sum_{k \geq 0} \left(D_{\delta_R,i} D_{\delta_L,i} \right)^k
\end{aligned}$$

Figure 19: Structure of the chains of type 5.

The structure of the others chains can then be deduced from the type 5 chains and is shown in Figure 20.

$$\begin{aligned}
C_{4R,i} &= D_{\delta_R,i} C_{5R,i} = C_{5L,i} D_{\delta_R,i} \\
C_{4L,i} &= D_{\delta_L,i} C_{5L,i} = C_{5R,i} D_{\delta_L,i}
\end{aligned}$$

Figure 20: Structure of the chains of type 4.

The generating functions of family B chains write:

$$\begin{aligned}
C_{5L} = C_{5R} &= D_{\delta_L} D_{\delta_R} \sum_{k \geq 0} (D_{\delta_L} D_{\delta_R})^k = \frac{D_{\delta_L} D_{\delta_R}}{1 - D_{\delta_L} D_{\delta_R}}, \\
C_{4L} &= D_{\delta_L} C_{5L} = \frac{D_{\delta_L}^2 D_{\delta_R}}{1 - D_{\delta_L} D_{\delta_R}}, \\
C_{4R} &= D_{\delta_R} C_{5R} = \frac{D_{\delta_L} D_{\delta_R}^2}{1 - D_{\delta_L} D_{\delta_R}}.
\end{aligned} \tag{35}$$

Using a similar argument as in the case of family A chains, the broken chains of this family are found to be

$$\begin{aligned}
B_{5L} = B_{5R} &= D_{\delta_L} D_{\delta_R} \frac{6 + 18D_{\delta_L} D_{\delta_R}}{(1 - D_{\delta_L} D_{\delta_R})(1 - 9D_{\delta_L} D_{\delta_R})}, \\
B_{4L} &= \frac{24D_{\delta_L}^2 D_{\delta_R}}{(1 - D_{\delta_L} D_{\delta_R})(1 - 9D_{\delta_L} D_{\delta_R})}, \\
B_{4R} &= \frac{24D_{\delta_L} D_{\delta_R}^2}{(1 - D_{\delta_L} D_{\delta_R})(1 - 9D_{\delta_L} D_{\delta_R})}.
\end{aligned} \tag{36}$$

The formulas obtained above for the generating functions of the various types of chains have therefore five different types of singular points:

- As any dipole has the same singular points as the melons, the chains also have the same singular points as the melons.
- For the unbroken and broken chains of family A, the points satisfying $D_\alpha + D_{\beta_L}D_{\beta_R} = 1$ are singular points.
- For the broken chains of family A, the points satisfying $3D_\alpha + 9D_{\beta_L}D_{\beta_R} = 1$ are singular points.
- For the colored and broken chains of family B, the points satisfying $D_{\delta_L}D_{\delta_R} = 1$ are singular points.
- For the broken chains of family B, the points satisfying $9D_{\delta_L}D_{\delta_R} = 1$ are singular points.

Inserting the expression of the generating functions of the dipoles in the singularity conditions above, one has:

$$\begin{aligned}
\frac{2}{3}(M_T(t) - 1) + \frac{1}{9}(M_T(t) - 1)^2 &= 1, \\
2(M_T(t) - 1) + (M_T(t) - 1)^2 &= 1, \\
\frac{1}{9}(M_T(t) - 1)^2 &= 1, \\
(M_T(t) - 1)^2 &= 1.
\end{aligned} \tag{37}$$

Each condition leads to a 2^{nd} order equation and the solutions of these equations are: $M_T = -2 \pm 3\sqrt{2}$, $M_T = \pm\sqrt{2}$, $M_T = 4$, -2 and resp. $M_T = 2$, 0 . The points where $3D_\alpha + 9D_\beta^2 = 1$ are therefore also points where the melons are singular. Recall that $M_T(t)$ was chosen to be an increasing function of t . This means that the singularity with the smallest $|M_T|$ is also the one with t closest to zero. Inserting $M_T = 0$ in equation (14) gives $1 = 0$ and is therefore impossible. The dominant singularity is then the point $(M_{T,c}, t_c) = (\sqrt{2}, \frac{1}{8\sqrt{2}+12})$ which is a singular point for the generating functions of melons and broken chains of family A.

Notice also from equation (34) that only the broken chains of type $2_L, 2_R, 3$ that are composed of a broken chain of type 1 are singular at the critical point. We denote these specific chains by a star such that $B_{2_L^*} = 3D_{\beta_L}B_1$, $B_{2_R^*} = 3D_{\beta_R}B_1$ and $B_{3^*} = 9D_{\beta_L}B_1D_{\beta_R}$.

Then, near the critical point, one gets:

$$\begin{aligned}
B_1 &\stackrel{t \rightarrow t_c}{\approx} \frac{3D_\alpha + 9D_\beta^2}{1 - (3D_\alpha + 9D_\beta^2)} \stackrel{t \rightarrow t_c}{\approx} \frac{1}{2M_{T,c}K\sqrt{1 - \frac{t}{t_c}}}, \\
B_{2_L} &\stackrel{t \rightarrow t_c}{\approx} B_{2_L^*} = 3D_{\beta_L}B_1 \stackrel{t \rightarrow t_c}{\approx} \frac{M_{T,c} - 1}{M_{T,c}K\sqrt{1 - \frac{t}{t_c}}}, \\
B_{2_R} &\stackrel{t \rightarrow t_c}{\approx} B_{2_R^*} = 3D_{\beta_R}B_1 \stackrel{t \rightarrow t_c}{\approx} \frac{M_{T,c} - 1}{M_{T,c}K\sqrt{1 - \frac{t}{t_c}}}, \\
B_3 &\stackrel{t \rightarrow t_c}{\approx} B_{3^*} = 9D_{\beta_L}D_{\beta_R}B_1 \stackrel{t \rightarrow t_c}{\approx} \frac{(M_{T,c} - 1)^2}{M_{T,c}K\sqrt{1 - \frac{t}{t_c}}}.
\end{aligned} \tag{38}$$

6.3 Scheme decomposition

As in [20] [33], the scheme \mathcal{S} of a graph \mathcal{G} is defined by eliminating from the respective graph any 2-point melonic subgraph, and replacing each maximal chain by its corresponding chain-vertex and any dipole by its corresponding dipole-vertex.

If a scheme is derived from a rooted graph, then the respective scheme naturally contains a rooted edge.

One can prove that the degree of the scheme $\omega(\mathcal{S})$ is identical to the one of the initial graph $\omega(\mathcal{G})$ (see again [20] [33]).

Each scheme represents then a family of graphs and any graph can be derived from its corresponding scheme by replacing/inserting back the corresponding dipoles, chains and melons.

Let us give an example of a scheme and a rooted Feynman graph corresponding to it in Fig. 21.

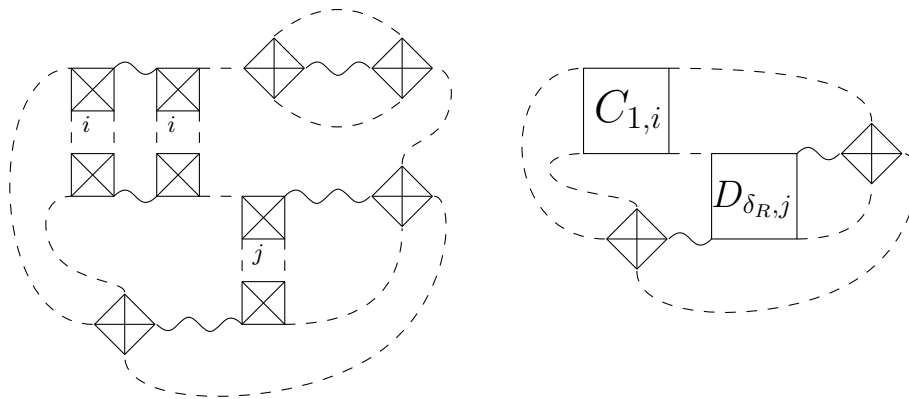


Figure 21: Example of a graph (left) and its corresponding scheme (right).

In [20] it was proven that the number of schemes at a given degree is finite in the $O(N)^3$ -invariant model. In order to obtain this result, it was proven that both the number of dipole/chain-vertices and the number of tetrahedric vertices was bounded.

The schemes of the prismatic model can be obtained by decorating the edge that links pairs of vertices of the schemes present in the tetrahedric model. There is also only a finite number of ways to perform such decoration on a scheme with a given number of dipole-vertices, chain-vertices, and tetrahedric vertices. This implies that the number of schemes at a given degree in the prismatic model must be finite.

As the number of schemes at each degree is finite, we can use them to compact the infinite number of graphs at a fixed degree into a finite number of schemes. Thus, the sum over an infinite number of Feynman graphs in $G_2(t)$ can be written as a sum over a finite number of schemes. The 2-point function then writes

$$G_2(t) = M_T(t) + \sum_{\omega \geq 1} N^{-\omega} \sum P_{\mathcal{S},\omega}(M, C), \quad (39)$$

where $P_{\mathcal{S},\omega}(M, C)$ is a polynomial of the melons generating function and the chains generating functions. The sum in the formula above is performed on all the schemes of degree ω . The dominant singularity of $G_2(t)$ is then the singular point $(M_{T,c}, t_c) = (\sqrt{2}, \frac{1}{8\sqrt{2}+12})$ of the broken chains of type $1, 2_L^*, 2_R^*$ and 3^* .

Dipole/chain-vertex removal When studying the combinatorics schemes, a standard operation is to remove dipole/chain-vertices and to reconnect the half-edges together on each sides of the vertices as in Figure 22.

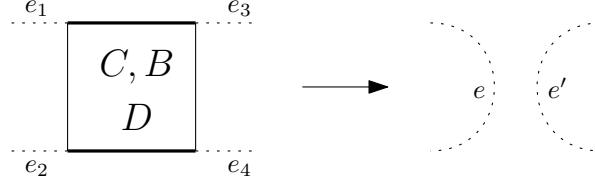


Figure 22: The process of dipole removal.

A dipole/chain-vertex is said to be separating if its removal disconnects the scheme \mathcal{S} . One can prove that the removal of a separating dipole/chain-vertex leads to a distribution of the degree between the two connected components (see again [20] and [33]). Thus, removing a separating dipole/chain-vertex leaves the degree invariant. Moreover, one has

$$\omega(\mathcal{S}) = \omega(\mathcal{S}_1) + \omega(\mathcal{S}_2), \quad (40)$$

where \mathcal{S}_1 and \mathcal{S}_2 are the two connected components resulting from the removal.

Let us denote by \mathcal{S}' the scheme obtained after a dipole removal in \mathcal{S} . By carefully counting the number of faces and vertices, one can prove (see again [20] and [33]) that removing a non separating dipole or chain of color i changes the degree as

$$\omega(\mathcal{S}) - 1 \geq \omega(\mathcal{S}') \geq \omega(\mathcal{S}) - 3. \quad (41)$$

Analogously, removing a non separating broken chain gives $\omega(\mathcal{S}') = \omega(\mathcal{S}) - 3$

Following [20], let us give here some details on the proof of the (40) and (41). Recall that changing the length of a chain doesn't change the degree of a scheme. Therefore, when studying the face structure of chains, one can consider the minimal case that are chains of length 2.

Separating dipole/chain-vertex. If a scheme \mathcal{S} possesses a separating dipole/chain-vertex, it is of one of the forms given in Figure 23, where the edges are either χ or T propagators. The scheme has then two 2-edge cuts at each side of the dipole/chain-vertex. Performing the two cuts leads to a new scheme \mathcal{S}' with 3 disconnected components, denoted by \mathcal{S}_0 , \mathcal{S}_1 , \mathcal{S}_2 , as given in Figure 24. The number of faces of \mathcal{S}' is $f_{\mathcal{S}'} = f_{\mathcal{S}_1} + f_{\mathcal{S}_2} + f_{\mathcal{S}_0} = f_{\mathcal{S}} + 6$ and the number of vertices $n_{\mathcal{S}'}$ is equal to $n_{\mathcal{S}}$. The degree $\omega(\mathcal{S})$ then writes:

$$\omega(\mathcal{S}) = 3 + n_{\mathcal{S}} - f_{\mathcal{S}} = 3 + n_{\mathcal{S}_1} + n_{\mathcal{S}_2} + n_{\mathcal{S}_0} - f_{\mathcal{S}_1} - f_{\mathcal{S}_2} - f_{\mathcal{S}_0} + 6 .$$

This can be rewritten as

$$\omega(\mathcal{S}) = \omega(\mathcal{S}_1) + \omega(\mathcal{S}_2) + \omega(\mathcal{S}_0) ,$$

and since the component \mathcal{S}_0 is a degree 0 component it gives:

$$\omega(\mathcal{S}) = \omega(\mathcal{S}_1) + \omega(\mathcal{S}_2) .$$

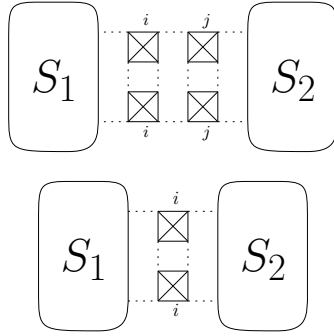


Figure 23: Structure of a scheme possessing a separating dipole/chain-vertex.

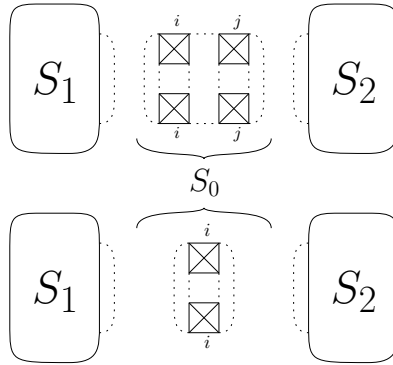


Figure 24: The three components that can be obtained from Figure 23.

Non-separating dipole vertex. In the case of a color i dipole only the faces of color i are affected by the removal. There are either 1 or 2 faces of color i adjacent to such dipoles as shown in Figure 25. Removing the dipole reduces the number of vertices by 2, and the number of faces by either 0, 1 or 2. This implies that, for a non-separating dipole removal, the variation of the degree $\Delta\omega$ is

$$-3 \leq \Delta\omega \leq -1 .$$

Non-separating chain vertex. When removing a chain vertex, one needs to separate the broken case to the colored one. If the chain is broken, the chains incident to the vertex are not affected by the removal. One can then count the variation of the number of internal faces and of vertices to obtain the variation of the degree. Doing so on the case of a chain of length 2 gives

$$\Delta\omega = 3 .$$

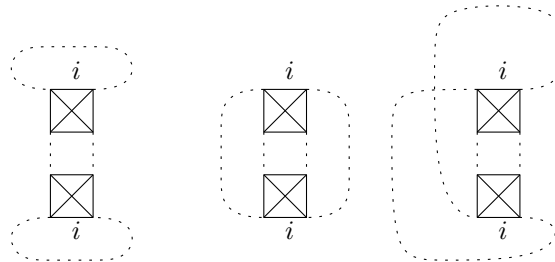


Figure 25: The three possible structures of the faces of color i adjacent to a color i dipole.

If the chain is not broken, the analysis is the same as the case of a non separating dipole removal, leading to

$$-3 \leq \Delta\omega \leq -1 .$$

Skeleton graphs When identifying the dominant schemes, a key role is played by skeleton graphs (see again [20]). These graphs are defined as follows.

Consider a scheme \mathcal{S} , its skeleton graph $\mathcal{I}(\mathcal{S})$ is obtained by removing all its broken chain-vertices of type 1 and by adding arrows (labeled by B_1) between the edges formed in this way. Notice that the definition given here is slightly different than the one given in [20].

Again, if the skeleton graph is built from a rooted scheme, it will also contain a root.

An example of such a dipole-vertex removal is given in Figure 26. In a skeleton graph, the arrows play the role of the edges whereas the disconnected components \mathcal{S}_i , resulting from the removals, play the role of the vertices. However, these edges and vertices don't contribute to the degree as in a Feynman graph. An example of a scheme and its skeleton graph is given in Figure 27.

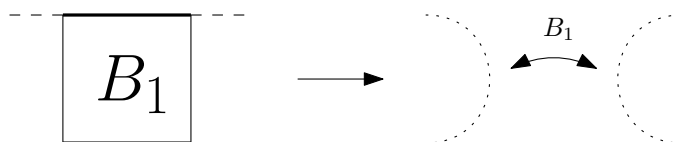


Figure 26: The dipole removal in the construction of the skeleton graph.

Skeleton graphs have several interesting properties (see again [20]):

- If one of the components \mathcal{S}_i has degree 0, then this component has a valency greater or equal to 3.

This can be proven by noticing that a degree 0 graph with valency 1 must be a melonic 2-point function and one with valency 2 must be a dipole or chain. None of these situations can occur for a skeleton graph.

- Let \mathcal{S} be a scheme with q non separating chain-vertices of type 1 and let \mathcal{S}' the scheme obtained by removing these q chain-vertices. The skeleton graph $\mathcal{I}(\mathcal{S}')$ is a tree and its degree satisfies the inequality: $\omega(\mathcal{I}(\mathcal{S})) \leq \omega(\mathcal{S}) - q$.

This comes from the fact that, if a scheme has only separating dipole/chain-vertices no cycle can appear in its skeleton graph. The bound on $\omega(\mathcal{I}(\mathcal{S}))$ is derived by using equation (41) and by recalling that the removal of a separating dipole/chain-vertex doesn't change the degree.

- If $\mathcal{I}(\mathcal{S})$ is a tree, its degree is equal to the one of its scheme and is given by the sum of the degree of its components

$$\omega(\mathcal{I}(\mathcal{S})) = \sum_i \omega(\mathcal{S}_i). \quad (42)$$

This comes from the fact that, if $\mathcal{I}(\mathcal{S})$ is a tree, all its dipole/chain-vertices are separating. This is then a direct consequence of equation (40).

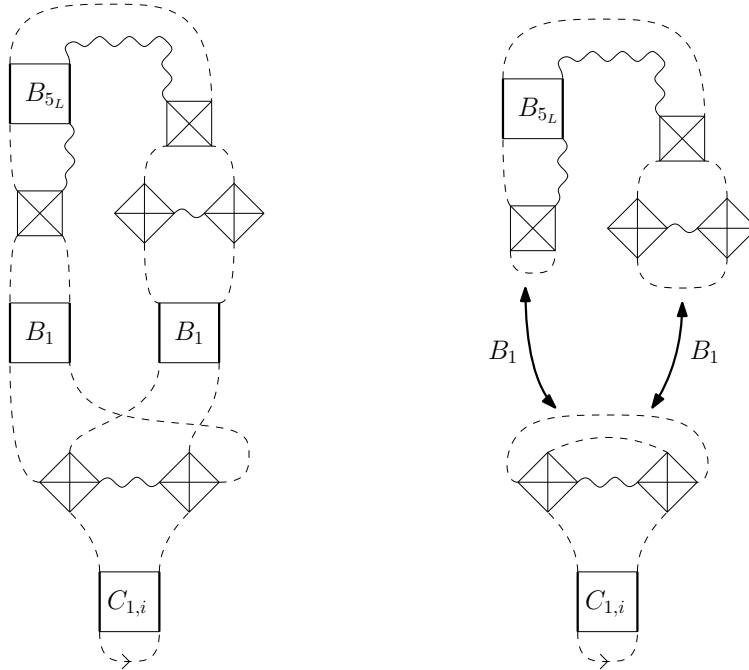


Figure 27: An example of a scheme and its skeleton graph.

7 Next-to-leading order graphs

In this section we explicitly identify the NLO Feynman graphs of the prismatic model. Recall from equation (11) that the degree of the prismatic model is a non-negative integer. Hence, if \mathcal{G} is an NLO Feynman graph, one has: $\omega(\mathcal{G}) = 1$.

The graphs of degree one for the tetrahedric model have been identified in [21]. Using this analysis, one can derive the corresponding NLO Feynman graphs of the model considered here. This is done using the following strategy. We consider all the graphs of degree one identified in [21], and investigate all the ways to decorate each graph with a χ propagator per pair of vertices. Finally, by contracting the intermediate field propagator χ and discarding the potential redundancies, all the graphs of degree one in the prismatic representation are found.

In the tetrahedric representation, the NLO graphs can be separated into three classes (see again [21]):

1. 2PI, dipole-free Feynman graphs
2. 2PI Feynman graphs with dipoles
3. 2PR Feynman graphs

In the sequel, we give the schemes of the graphs in the tetrahedric representation and give some examples of Feynman graphs in both the tetrahedric and the prismatic representations. Recall that the number of tetrahedric vertices replacing a chain-vertex is arbitrary, and the same holds for the corresponding number prismatic vertices (when using the prismatic representation of the model).

7.1 Dipole-free 2 particle irreducible graphs

It was derived in [21] that there is a unique dipole free scheme of degree one in the tetrahedric model. This scheme is given in Figure (28).

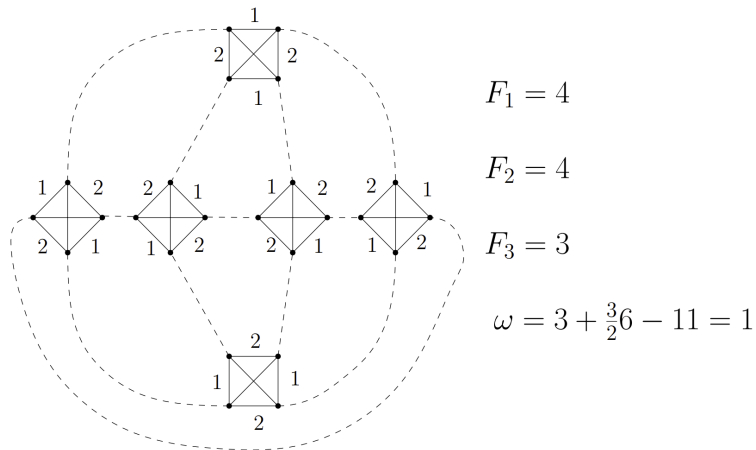


Figure 28: The unique 2PI dipole free scheme of degree one in the tetrahedric model.

Note that, since this scheme has no dipole-vertices and no chain-vertices, one can obtain the corresponding graphs by the usual melonic insertions on any of its edges.

There are then 3 independent ways to place the χ propagator on this NLO graph, see Fig. 29.

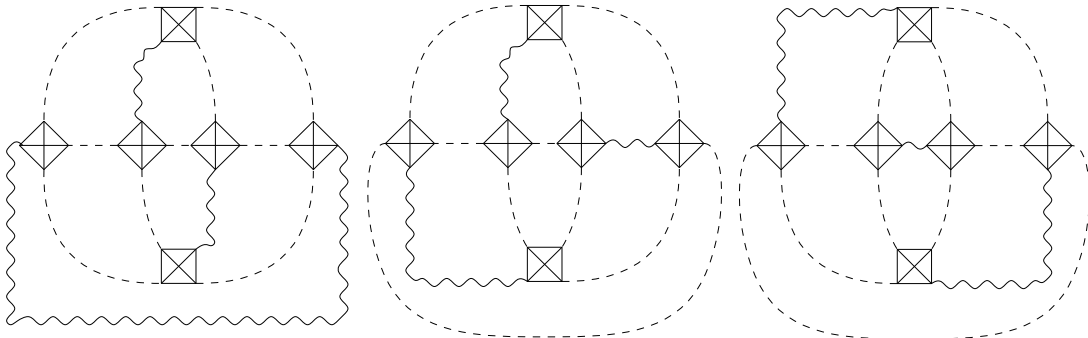


Figure 29: The different ways to place the χ propagators on the NLO graph of Fig. 28.

However, when contracting the χ propagators in order to obtain the prismatic representation NLO graphs, one can show that the three graphs of Fig. 29 lead to the unique graph of Fig. 30.

The NLO graphs in the prismatic representation are thus obtained *via* the two prismatic melonic moves (see above) performed on the graph of Fig. 30.

7.2 2PI graphs with dipoles

The schemes of the 2PI graphs with dipoles in the tetrahedric representation are given in Figure 31. The edges e and e' can be of type T or χ , implying that $s = 1$ or 5 (the case $s = 4$ being equivalent to $s = 1$). The explicit schemes, with the corresponding T or χ propagators, are given on the right side of Fig. 32.

Let us end this subsection by giving some explicit examples of NLO 2PI graphs with dipoles (where we have replaced the chain-vertices by chains of length four), and their corresponding graphs in the prismatic representation - see Figure 33.

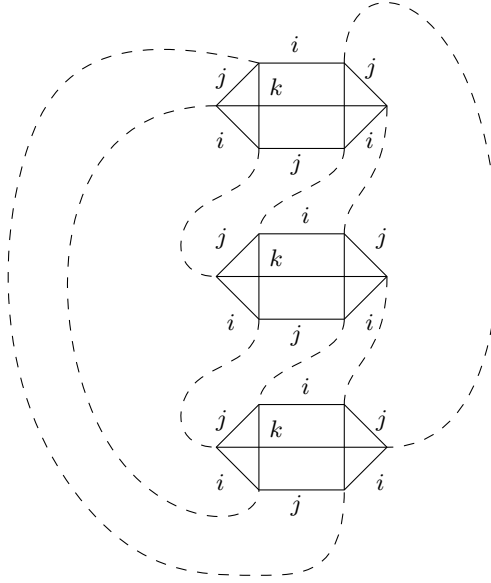


Figure 30: The only graph found by contracting the χ edges of the graphs in Figure 28.

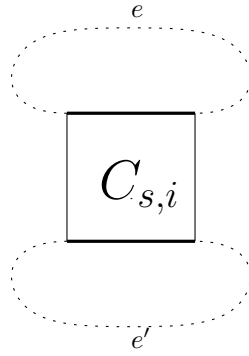


Figure 31: The explicit schemes of the 2PI NLO graphs with dipoles.

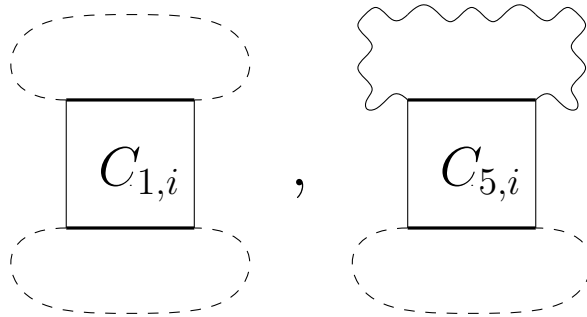


Figure 32: The explicit schemes of the 2PI NLO graphs with dipoles.

7.3 2 particle reducible NLO graphs

Recall from [21] that schemes of the 2PR graphs in the tetrahedric model are given in Fig. 34.

When placing the χ propagators, the corresponding schemes are given in Fig. 35. The empty boxes in the figures can either be a dipole-vertex, a broken chain-vertex or a colored chain-vertex.

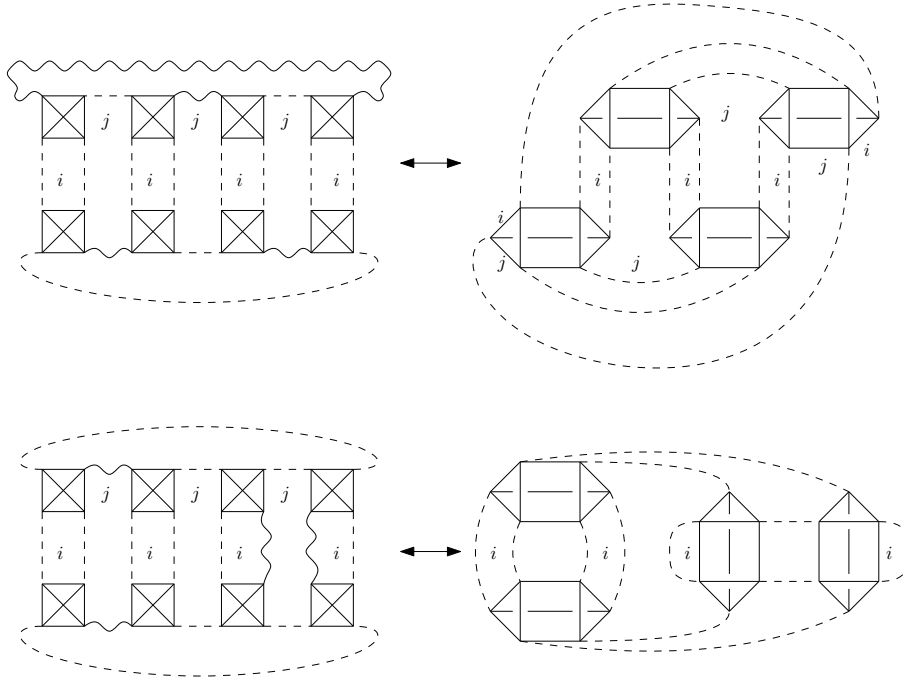


Figure 33: Examples of NLO, 2PI graphs with dipoles in the tetrahedric (left) and prismatic (right) representation.

Let us end this section by giving some examples of NLO 2PR graphs and the corresponding graph in the prismatic representation, see Figure 36. The first graph in the figure is the first graph of Fig. 35. The second graph is obtained from the second scheme of Fig. 35, where we have replaced the empty box by a chain of length four and color i . Finally, the third graph is obtained from the second scheme of Fig. 35, where we have replaced the empty box by a broken chain of length four.

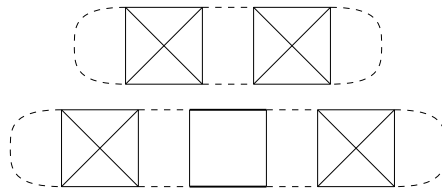


Figure 34: The schemes of the NLO 2PR graphs in the single field tetrahedric model.

8 Double scaling limit of the 2-point function

Let us recall that since we are aiming to compute $G_2(t, N)$, we are working with rooted objects. Moreover, the dominant singularity of $G_2(t, N)$ is the point $(M_{T,c}, t_c) = (\sqrt{2}, \frac{1}{8\sqrt{2+12}})$ where the broken chains of type 1, 2_L^* , 2_R^* and 3^* are singular. The dominant schemes are then the ones that maximize the number of these chains.

The general strategy used in this section is the following:

- we remove all the non separating dipole/chain-vertices of a scheme \mathcal{S} ; we denote by \mathcal{S}' the resulting scheme.

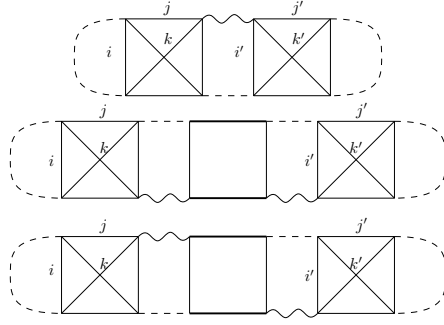


Figure 35: The schemes of the NLO 2PR graphs.

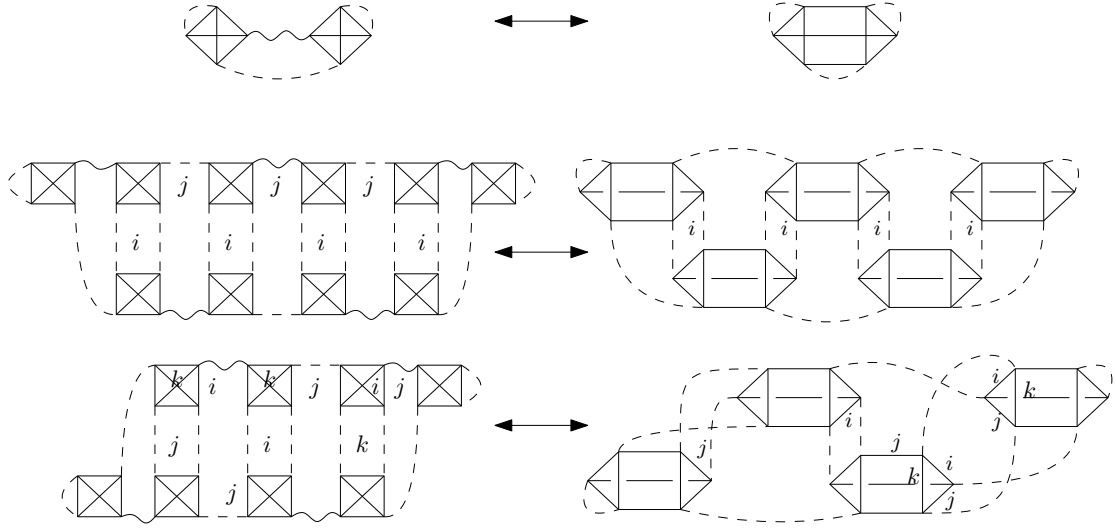


Figure 36: Examples of the degree 1, 2PR graphs in the tetrahedric (left) and the prismatic (right) representation.

- we derive different bounds on the number of components of \mathcal{S}'
- finally, we use these bounds to obtain appropriate bounds on the sum of number of broken chain-vertices of type 1, 2_L^* , 2_R^* and 3^* of the original scheme \mathcal{S} .

Thus, let us consider a scheme \mathcal{S} with b the sum of the number of broken chains of type 1, 2_L^* , 2_R^* , 3^* . Note that these broken chains can be separating or non-separating, and we denote by p and resp. q the number of separating and resp. non-separating broken chains:

$$b = p + q. \quad (43)$$

We need to find a bound on b . In order to do so, as explained above, we remove all the q non-separating broken chain-vertices and denote by \mathcal{S}' the resulting scheme. The degree of \mathcal{S}' is then $\omega(\mathcal{S}') = \omega(\mathcal{S}) - 3q$, and the resulting scheme has p separating broken chains of type 1, 2_L^* , 2_R^* , 3^* . We then split every broken chain-vertex of type 2_L^* resp. 2_R^* into a dipole-vertex (of any color) of type β_L resp. β_R and a broken chain-vertex of type 1. Similarly, we split every broken chains-vertex of type 3^* into two dipoles vertices of type β and a broken chain-vertex of type 1. The graphical representation of this splitting procedure is given in Figure 37. After this splitting, the scheme \mathcal{S}' has p separating broken chains-vertices of type 1.

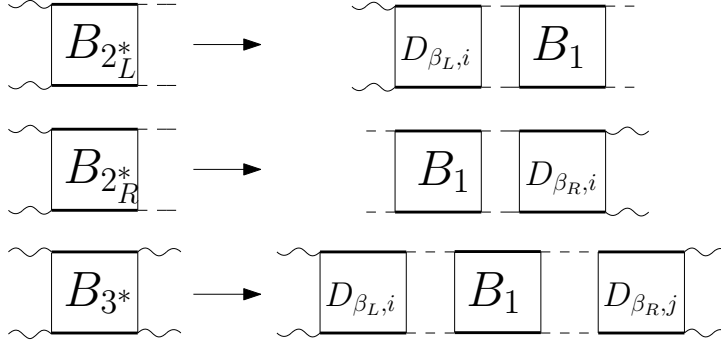


Figure 37: Splitting of the chains of type 2^* , 3^* .

Consider the skeleton graphs $\mathcal{I}(\mathcal{S}')$ of \mathcal{S}' . As \mathcal{S}' had only separating broken chains, $\mathcal{I}(\mathcal{S}')$ is a tree and its degree is given by the sum of the degree of its components. Recall that the smallest positive degree possible for the components of $\mathcal{I}(\mathcal{S}')$ is one.

Since we are studying the 2–point function, the skeleton graph $\mathcal{I}(\mathcal{S}')$ possesses a root and has 3 types of connected components:

- The rooted component, it is unique.
- Non rooted components of positive degree, we denote their number by N_+ .
- Non-rooted components of degree zero. Such components are said to be *tracked* if they are connected to a non separating broken chain-vertex of type 1 in \mathcal{S} . Otherwise the components are said to be non-tracked. The number of non rooted degree 0 components is denoted by $N_0 = N_{0,t} + N_{0,nt}$ where $N_{0,t}$ resp. $N_{0,nt}$ is the number of tracked resp. non-tracked non-rooted degree 0 components.

Therefore, the number of components N_c of the skeleton graph reads

$$N_c = N_{0,nt} + N_{0,t} + N_+ + 1. \quad (44)$$

Recall that in the skeleton graph $\mathcal{I}(\mathcal{S})$, a degree 0 component has a valency at least equal to three. This implies that in $\mathcal{I}(\mathcal{S}')$ the valency of a tracked degree component is at least equal to one since it is at most connected to two separating broken chain-vertices of type 1 in \mathcal{S} .

Following [20], one can prove the following bounds:

$$N_{0,t} \leq 2q, \quad (45)$$

$$N_+ \leq \omega(\mathcal{S}'), \quad (46)$$

$$2p \geq 3N_{0,nt} + N_{0,t} + N_+ + 1, \quad (47)$$

$$p = N_{0,nt} + N_{0,t} + N_+. \quad (48)$$

After some algebra, one gets the following inequality

$$p \leq 2\omega(\mathcal{S}') + 4q - 1,$$

using $\omega(\mathcal{S}') = \omega(\mathcal{S}) - 3q$ one gets

$$p \leq 2\omega(\mathcal{S}) - 2q - 1, \quad (49)$$

which further leads to:

$$b \leq 2\omega(\mathcal{S}) - q - 1. \quad (50)$$

Hence the maximal value for b is $2\omega(\mathcal{S}) - 1$ (when $q = 0$). One can check that when b reaches the upper bound, the inequalities (45), (46) and (47) turn into equalities. This implies that $N_{0,t} = 0$, $N_+ = \omega(\mathcal{S})$ and that the valency of all degree 0 components is 3, while the one of the positive degree components is 1.

All positive components in $\mathcal{I}(\mathcal{S}')$ are of degree one, hence there are two possibilities. The components connected to a broken chain of type 1, 2_L^* or 2_R^* (on the T propagator side) before the removal are given by the NLO schemes described in Section 7.

The components that are connected to a broken chain of type 3^* , 2_L^* or 2_R^* (on the χ propagator side) are the NLO schemes described in Section 7 with a 2-point graph (obtained from the contraction of a dipole of type β_L or β_R as shown in Figure 38) inserted in any of their χ propagator.

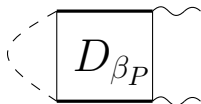


Figure 38: Contraction of a type β dipole leading to a 2-point graph. ($P = L$ or R)

The degree 0 components are all non tracked and have adjacency 3. They must then come from schemes of the form given by Figure 39 where $s = 1, 2_L^*, 2_R^*, 3^*$.

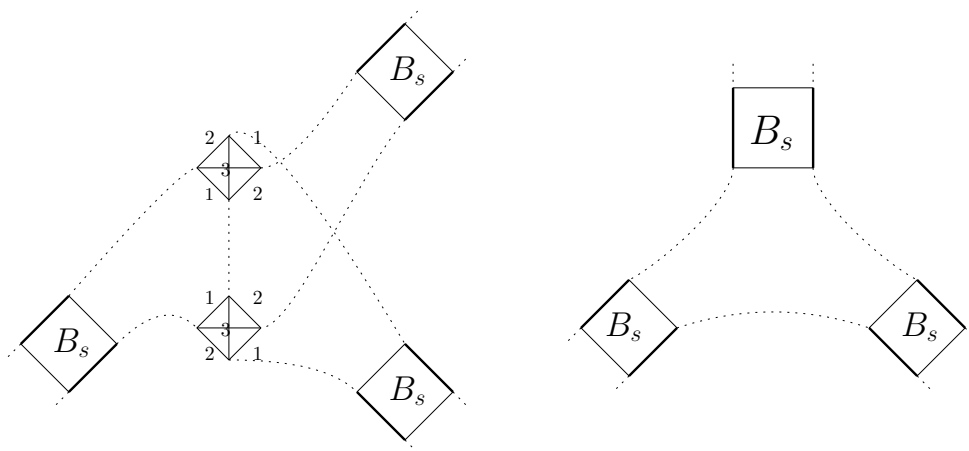


Figure 39: The different subschemes that can produce a component of degree 0 and adjacency 3 in the skeleton graph. $B_{t,A}$ can be any broken chain of type $s = 1, 2_L^*, 2_R^*, 3^*$ and family A.

Finally, following [20], one gets that the skeleton graph $\mathcal{I}(\mathcal{S}')$ is a rooted binary tree with $\omega(\mathcal{S})$ leaves given by the rooted component or the degree 1 components and $\omega(\mathcal{S}) - 1$ inner nodes given by components of degree 0.

As the schemes are fully encoded by their skeleton graphs, the dominant schemes are thus in bijection with the rooted binary trees described above.

The generating function of these trees is

$$G_{\omega, \mathcal{T}}(t) = B_1(t)^{2\omega-1} I(t)^{\omega-1} L(t)^\omega, \quad (51)$$

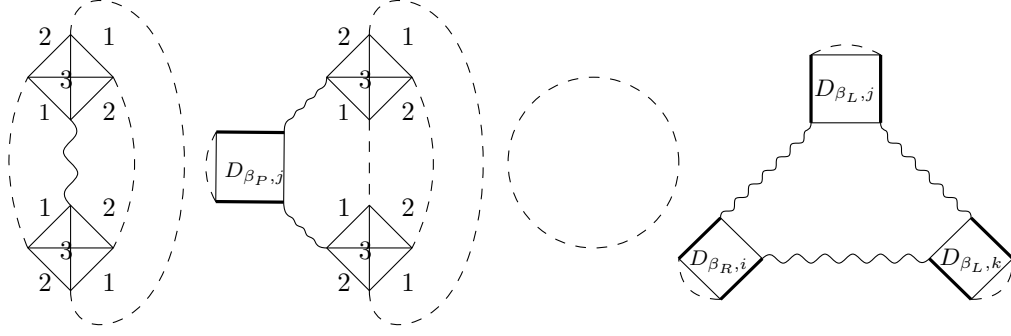


Figure 40: The internal nodes of $\mathcal{I}'(\mathcal{S}')$

where $I(t)$ resp. $L(t)$ are the weights coming from the internal nodes resp. leaves.

The expression of $L(t)$ is derived by considering all the 2-point subschemes that lead to a component of degree and valency 1 in the skeleton graphs $\mathcal{I}'(\mathcal{S})$ of the scheme \mathcal{S} . There is a consequent number of such subschemes, hence $L(t)$ will be the sum of a consequent number of terms coming from these subschemes. By a tedious but straightforward computation, one finds the following expressions:

$$\begin{aligned} I(t) &= 6tM_T(t)^3M_\chi(t)(1 + 3D_\beta) + 1 + (3D_\beta)^3, \\ &= 2(M_T(t) - 1)(1 + 3D_\beta) + 1 + (3D_\beta^3), \end{aligned} \quad (52)$$

$$\begin{aligned} L(t) &= 9M_T(t)^9M_\chi(t)^3(1 + D_\beta(t)) + 3C_1(t) + 6(C_1(t) + D_\alpha(t))M_T^3(t)M_\chi(t) \\ &\quad + 12(C_2(t) + D_\beta(t))M_T(t)^3M_\chi(t) + 3C_5(t) + 6(C_4(t) + D_\delta(t))M_T^3(t)M_\chi(t) \\ &\quad + 9D_\beta(t)C_5(t) + 9D_\beta(t)C_4(t) + 18C_1(t)M_T^3(t)M_\chi(t) \\ &\quad + M_T(t)^3M_\chi(t)\left[18 + 27D_\beta(t) + 54D_\beta(t) + 54C_4(t) + 18B_4(t) + 54C_5(t) \right. \\ &\quad \left. + 18B_5(t)\right] + M_T^3(t)M_\chi(t)27(1 + 3D_\beta(t))\left[3D_\beta^2(t) + 3D_\beta(t)(C_4(t) + C_5(t)) \right. \\ &\quad \left. + D_\beta(t)(B_4(t) + B_5(t)) + \frac{3}{2}(C_4^2(t) + C_5^2(t)) + 3C_4(t)C_5(t) \right. \\ &\quad \left. + C_4(t)B_5(t) + B_4(t)C_5(t)\right] + M_T^3(t)M_\chi(t)9(1 + 3D_\beta(t))(B_4^2(t) + B_5^2(t) \\ &\quad + B_4(t)B_5(t)) + 54M_T(t)^6M_\chi^2(t)\left[3D_\beta(t) + 3C_4(t) + B_4(t) + 3C_5(t) \right. \\ &\quad \left. + 3D_\beta(t)(3C_4(t) + 3D_\beta(t) + 3C_5(t) + B_4(t) + B_5(t)) + B_5(t) + 3C_4(t)(3C_5(t) \right. \\ &\quad \left. + \frac{3}{2}C_4(t) + B_4(t) + B_5(t)) + 3C_5(t)(\frac{3}{2}C_5(t) + B_4(t) + B_5(t))\right]. \end{aligned} \quad (53)$$

We can now sum over all the trees described above and add a melonic insertion at the root to find the generating function of the dominant Feynman graphs of a given degree ω

$$G_{\omega, \text{dom}}(t) = M_T(t) \sum_{\mathcal{T}} G_{\omega, \mathcal{T}} = M_T(t) \text{Cat}_{\omega-1} B_1(t)^{2\omega-1} I(t)^{\omega-1} L(t)^\omega, \quad (54)$$

where $\text{Cat}_{\omega-1}$ is the $(\omega - 1)^{\text{th}}$ Catalan number. Using equation (38) we find that

$$G_{\omega, \text{dom}} \stackrel{t \rightarrow t_c}{\sim} \text{Cat}_{\omega-1} M_{T,c} \left(\frac{1}{2M_{T,c}K\sqrt{1 - \frac{t}{t_c}}} \right)^{2\omega-1} I(t_c)^{\omega-1} L(t_c)^\omega. \quad (55)$$

Let us now define the double scaling parameter $\kappa(t, N)$ as

$$\kappa(t, N) = \frac{I(t_c)L(t_c)}{4NM_{T,c}^2K^2(1 - \frac{t}{t_c})}. \quad (56)$$

Recall that in the $\frac{1}{N}$ expansion, the Feynman amplitude of a generic vacuum graph of degree ω scales as $N^{3-\omega}$, and the one of a 2-point function graph hence scales as $N^{-\omega}$ (since, when cutting an edge of a vacuum graph in order to obtain a 2-point function graph, 3 faces, and hence a factor N^3 , are lost). The contribution of the dominant graphs of degree ω to the 2-point function in the double scaling limit then writes

$$N^{-\omega}G_{\omega,\text{dom}} = M_{T,c}N^{-1/2} \left(\frac{L(t_c)\kappa(t, N)}{I(t_c)} \right)^{1/2} \text{Cat}_{\omega-1}\kappa(t, N)^{\omega-1}. \quad (57)$$

Let us comment on the choice of double scaling parameter. In the expression of $N^{-\omega}G_{\omega,\text{dom}}$ above, we need only powers of ω as exponent of only the factor $\kappa(t, N)$ for two reasons. Firstly, we need all non-zero degree dominant graphs to contribute to the same power of N in the double scaling limit. Secondly, by choosing such a double scaling parameter one can sum over all degrees the factor $\text{Cat}_{\omega-1}\kappa(t, N)^{\omega-1}$ to obtain an exact expression for $\sum_{\omega>0} N^{-\omega}G_{\omega,\text{dom}}$ as given in equation (58) below.

Adding the contribution of the melons and summing over all the degrees, the 2-point function in the double scaling limit is

$$\begin{aligned} G_{2,DS}(t, N) &= M_{T,c} + \sum_{\omega>0} N^{-\omega}G_{\omega,\text{dom}} \\ &= M_{T,c} + M_{T,c}N^{-\frac{1}{2}} \left(\frac{L(t_c)\kappa(t, N)}{I(t_c)} \right)^{1/2} \sum_{\omega \in \mathbb{N}^*} \text{Cat}_{\omega-1}\kappa(t, N)^{\omega-1} \\ &= M_{T,c} \left(1 + N^{-\frac{1}{2}} \left(\frac{L(t_c)}{I(t_c)} \right)^{1/2} \frac{1 - \sqrt{1 - 4\kappa(t, N)}}{2\kappa(t, N)^{1/2}} \right) \end{aligned} \quad (58)$$

Let us end this section by giving some interpretation of the result above. One can see that, in the double scaling limit, the 2-point function picks up contributions of all degrees, and not just from the vanishing degree (as it is the case for the large N limit). Moreover, one can notice that the higher it is the degree of the graph, the greater it is the contribution from the respective degree when the coupling constant tends to the critical value. Note also that, in the limit $\kappa \rightarrow 0$ the large N limit is recovered. This behaviour is identical to the one of the matrix case.

As the sum in equation (58) is convergent for $\kappa \leq 1/4$, the double scaling limit series of the prismatic model is thus convergent. This is different from the matrix model case where the double scaling series diverge. The result obtained here is analogous to the one obtained for quartic tensor models (see again [20], [26] and [25]). Finally, let us mention that one could expect to obtain a similar double scaling limit behaviour for other sextic tensor models.

9 Free energy in the double scaling limit

In this section, starting from the double scaling limit of the 2-point function, we compute the free energy in the double scaling limit .

Recall the relation between the free energy and the 2–point function

$$F(t, N) = \tilde{F}(s = 1, \tilde{t}, N) = - \int_0^1 \frac{ds}{2s} G_2(\tilde{t}s^3) .$$

Since \tilde{F} is evaluated at $s = 1$, taking the limit $t \rightarrow t_c$ is equivalent to taking $\tilde{t} \rightarrow t_c$. Recall also that the 2–point function can be written as

$$G_2(t) = M_T(t) + \sum_{\omega > 0} N^{-\omega} G_\omega .$$

The free energy then writes:

$$F(t, N) = - \int_0^1 \frac{ds}{2s} M_T(s^3 \tilde{t}) - \sum_{\omega} \int_0^1 \frac{ds}{2s} N^{-\omega} G_\omega(s^3 \tilde{t}) .$$

The first term in the equation above is the leading order contribution that we denote by $F_{LO}(t)$. The second term can be computed in the double scaling limit. In this limit only the part of the integral close to one and the dominant graphs contribute to $F(t, N)$. Let us denote by ϵ a small and fixed quantity. We split the second term as

$$- \sum_{\omega} N^{-\omega} \int_{1-\epsilon}^1 \frac{ds}{2s} G_\omega(s^3 \tilde{t}) - \sum_{\omega} N^{-\omega} \int_0^{1-\epsilon} \frac{ds}{2s} G_\omega(s^3 \tilde{t})$$

and we are only interested in the first term above and in the contribution of the dominant graphs $G_{\omega, dom}$. Since the limit $\tilde{t} \rightarrow t_c$ is taken we can use equation (55) to rewrite the integral:

$$- \sum_{\omega} \int_{1-\epsilon}^1 \frac{ds}{2s} G_\omega(s^3 \tilde{t}) \stackrel{t \rightarrow t_c}{\sim} - \sum_{\omega} \text{Cat}_{\omega-1} \frac{M_{T,c} I(t_c)^{\omega-1} L(t_c)^{\omega}}{(2M_{T,c} K)^{2\omega-1}} \int_{1-\epsilon}^1 \frac{ds}{2s} \left(1 - \frac{s^3 \tilde{t}}{t_c}\right)^{1/2-\omega} .$$

Using the change of variables $u = s^3$ and $v = 1 - u \frac{\tilde{t}}{t_c}$ we find

$$\int_{1-\epsilon}^1 \frac{ds}{2s} \left(1 - \frac{s^3 \tilde{t}}{t_c}\right)^{1/2-\omega} = \frac{3}{2} \int_{1-\frac{\tilde{t}}{t_c}}^{1-(1-\epsilon)^3 \frac{\tilde{t}}{t_c}} dv \frac{v^{1/2-\omega}}{1-v} .$$

We can expand $\frac{1}{1-v}$ as

$$\frac{1}{1-v} \approx \sum_n \left(\frac{t_c}{\tilde{t}}\right)^{n+1} v^n .$$

The integral is then evaluated as

$$\frac{3}{2} \int_{1-\frac{\tilde{t}}{t_c}}^{1-(1-\epsilon)^3 \frac{\tilde{t}}{t_c}} dv \frac{v^{1/2-\omega}}{1-v} = \sum_n \frac{3}{2(3/2 - \omega + n)} \left(\frac{t_c}{\tilde{t}}\right)^{n+1} \left[v^{3/2-\omega+n} \right]_{1-\frac{\tilde{t}}{t_c}}^{1-(1-\epsilon)^3 \frac{\tilde{t}}{t_c}} .$$

In the limit $\tilde{t} \rightarrow t_c$, the most divergent contribution is given by the term $n = 0$ at $v = 1 - \frac{\tilde{t}}{t_c}$. We thus have

$$- \sum_{\omega} N^{-\omega} \int_{1-\epsilon}^1 \frac{ds}{2s} G_\omega(s^3 \tilde{t}) \stackrel{\tilde{t} \rightarrow t_c}{\sim} \sum_{\omega} N^{-\omega} \text{Cat}_{\omega-1} \frac{M_{T,c} I(t_c)^{\omega-1} L(t_c)^{\omega}}{(2M_{T,c} K)^{2\omega-1}} \frac{\left(1 - \frac{t}{t_c}\right)^{3/2-\omega}}{(1 - 2/3\omega)} ,$$

which can be rewritten using the definition of the double scaling parameter (56) as:

$$- \sum_{\omega} N^{-\omega} \int_{1-\epsilon}^1 \frac{ds}{2s} G_\omega(s^3 \tilde{t}) \stackrel{\tilde{t} \rightarrow t_c}{\sim} \frac{N^{-3/2} I(t_c)^{1/2} L(t_c)^{3/2}}{4M_{T,c} K^2 \kappa(t, N)^{1/2}} \sum_{\omega} \text{Cat}_{\omega-1} \frac{\kappa(t, N)^{\omega-1}}{(1 - 2/3\omega)} .$$

We thus conclude that the free energy in the double scaling limit is given by:

$$F_{DS}(t, N) = F_{LO,c} + \frac{N^{-3/2} I(t_c)^{1/2} L(t_c)^{3/2}}{4M_{T,c} K^2 \kappa(t, N)^{1/2}} \sum_{\omega} \text{Cat}_{\omega-1} \frac{\kappa(t, N)^{\omega-1}}{\left(1 - \frac{2}{3}\omega\right)},$$

where $F_{LO,c}$ is the value of $F_{LO}(t)$ at $t = t_c$.

10 Concluding remarks

In this paper, we studied the double scaling limit of the $O(N)^3$ invariant-tensor model with a sextic prismatic interaction. Using the intermediate field method, this sextic interaction has been reduced to a quartic $T^3\chi$ tetrahedric one, χ being the intermediate field. This method allowed us to work in the so-called tetrahedric representation where all prismatic vertices of the Feynman graphs are split in pairs of tetrahedra vertices. In order to obtain our results, we thus generalised the methods used in the study of the single field model with T^4 tetrahedric interaction to the $T^3\chi$ case.

This strategy allowed us to give a new method to identify the LO graphs explicitly in the large N expansion of the model. In the tetrahedric representation, the LO graphs are melonic graphs with melonic insertions that can be performed on the two types of propagators. In the prismatic representation, the LO graphs are a different class of graphs. These graphs are obtained from the triple tadpole given in Figure 8 and recursively inserting a 2-point double tadpole on any propagator or splitting any prismatic vertex into two such vertices linked by a pair of edges as in Figure 9. We have then have introduced chains, dipoles and schemes and we used them to describe the general terms of the $1/N$ expansion of the model. We used them to exhibit both the NLO and the dominant graphs of the model in the tetrahedric representation. The schemes of the dominant graphs are in bijection with rooted binary trees whose leaves are the schemes of the NLO graphs and whose internal nodes are degree 0 components. Finally, we computed the 2-point function in the double scaling limit, see equation (58) above.

A natural follow up is to apply methods used in this paper to other sextic interactions, such as the sextic interactions considered (from a renormalization perspective) in [22]. For example, one could consider a model with the four interactions given in Figure 41. By using a real intermediate field, the interactions of the model can be

Figure 41: The internal nodes of $\mathcal{T}'(\mathcal{S}')$

reduced to a tetrahedric and pillows $T^3\chi$ interactions as in Figure 42. In this model, the tetrahedron interactions can be paired to pillow interactions. This renders the model somehow richer than the prismatic model with a more envolved combinatorial structure. Moreover, the study of this model could serve as an intermediate step toward the computation of the double scaling limit of the $O(N)^3$ -invariant tensor model containing all the sextic connected interactions.

Remark that this model is not the most general as one could consider the same interaction with distinct coupling constants for each interacting term. In this case, one would need to use both real and complex intermediate fields to express all the sextic interactions in a quartic representation. The presence of both complex and real intermediate fields would thus lead to further complications of the analysis given in this paper.

$$\sqrt{\lambda_1} \begin{array}{c} T \\ \diagup \quad \diagdown \\ \chi_t \\ \diagdown \quad \diagup \\ T \end{array} + \sqrt{\lambda_2} \sum_{i=1}^3 \begin{array}{c} T \quad i \quad T \\ \diagup \quad \quad \diagdown \\ \chi_p \quad i \quad T \\ \diagdown \quad \quad \diagup \end{array}$$

Figure 42: The internal nodes of $\mathcal{I}'(\mathcal{S}')$

Moreover, we would like to emphasize that our analysis is not limited to the interactions presented here. In a more general setting, one can define a separating D -cut as a cut of D colored edges that separates a bubble interaction into two disconnected components. Any interaction possessing a separating D -cut can be written in an intermediate form using a rank D intermediate field. This intermediate field is real if the two disconnected components are identical and complex otherwise. However, this representation may not be useful as it can lead to interactions that cannot be colored in a natural way or that can mix tensors of different ranks. When generalising the method described in this paper, one should restrict itself to interactions possessing cuts of the same rank as the one of the tensors in the initial action. An example of interaction on which our analysis is not directly applicable is the wheel (or $K(3, 3)$) interaction shown in Figure 43. This interaction possesses only separating 4-cuts (or higher) but is built out of rank 3 tensors.

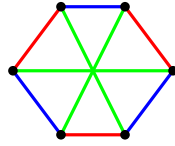


Figure 43: The wheel interaction.

Acknowledgements. The authors have been partially supported by the ANR-20-CE48-0018 “3DMaps” grant. A. T. has been partially supported by the PN 09370102 grant. The authors acknowledge support of the Institut Henri Poincaré (UAR 839 CNRS-Sorbonne Université), and LabEx CARMIN (ANR-10-LABX-59-01). The authors warmly acknowledge Victor Nador for useful discussions at various steps of this research project.

References

- [1] R. G. Gurau. *Random tensors*. Oxford University Press, 2017.
- [2] A. Tanasa. *Combinatorial Physics*. Oxford University Press, 2021.
- [3] A. Tanasa. “The Multi-Orientable Random Tensor Model, a Review”. In: *Symmetry, Integrability and Geometry: Methods and Applications* (June 2016). DOI: [10.3842/sigma.2016.056](https://doi.org/10.3842/sigma.2016.056).

- [4] A. Tanasa. “Tensor models, a quantum field theoretical particularization”. In: *Proc. Rom. Acad. A* 13.3 (2012), pp. 225–234. arXiv: [1211.4444 \[math.CO\]](#).
- [5] R. Gurau. *Notes on Tensor Models and Tensor Field Theories*. 2019. DOI: [10.48550/ARXIV.1907.03531](#).
- [6] R. G. Gurau. “Notes on tensor models and tensor field theories”. In: *Ann. Inst. H. Poincaré D Comb. Phys. Interact.* 9.1 (2022), pp. 159–218. DOI: [10.4171/aihpd/117](#). arXiv: [1907.03531 \[hep-th\]](#).
- [7] I. R. Klebanov, F. Popov, and G. Tarnopolsky. “TASI Lectures on Large N Tensor Models”. In: *PoS TASI2017* (2018), p. 004. DOI: [10.22323/1.305.0004](#). arXiv: [1808.09434 \[hep-th\]](#).
- [8] J.-B. Zuber. *Introduction to random matrices*. 2011.
- [9] P. Francesco, P. Ginsparg, and J. Zinn-Justin. “2D gravity and random matrices”. In: *Physics Reports* 254.1-2 (Mar. 1995), pp. 1–133. DOI: [10.1016/0370-1573\(94\)00084-g](#).
- [10] P. Di Francesco. *2D Quantum Gravity, Matrix Models and Graph Combinatorics*. 2004. DOI: [10.48550/ARXIV.MATH-PH/0406013](#).
- [11] E. Witten. *An SYK-Like Model Without Disorder*. 2016. DOI: [10.48550/ARXIV.1610.09758](#).
- [12] I. R. Klebanov and G. Tarnopolsky. “Uncolored random tensors, melon diagrams, and the Sachdev-Ye-Kitaev models”. In: *Phys. Rev. D* 95.4 (2017), p. 046004. DOI: [10.1103/PhysRevD.95.046004](#). arXiv: [1611.08915 \[hep-th\]](#).
- [13] Kitaev. <http://online.kitp.ucsb.edu/online/entangled15/kitaev/>, (talk at KITP).
- [14] J. Ambjørn, B. Durhuus, and T. Jónsson. “Three-Dimensional simplicial quantum gravity and generalized matrix models”. In: *Modern Physics Letters A* 06.12 (1991), pp. 1133–1146. DOI: [10.1142/S0217732391001184](#). eprint: <https://doi.org/10.1142/S0217732391001184>.
- [15] R. Gurau. “Colored Group Field Theory”. In: *Communications in Mathematical Physics* 304.1 (Mar. 2011), pp. 69–93. DOI: [10.1007/s00220-011-1226-9](#).
- [16] R. Gurau. “The $1/N$ Expansion of Colored Tensor Models”. In: *Annales Henri Poincaré* 12.5 (Mar. 2011), pp. 829–847. DOI: [10.1007/s00023-011-0101-8](#).
- [17] A. Tanasa. “Multi-orientable Group Field Theory”. In: *J. Phys. A* 45 (2012), p. 165401. DOI: [10.1088/1751-8113/45/16/165401](#). arXiv: [1109.0694 \[math.CO\]](#).
- [18] S. Dartois, V. Rivasseau, and A. Tanasa. “The $1/N$ Expansion of Multi-Orientable Random Tensor Models”. In: *Annales Henri Poincaré* 15.5 (June 2013), pp. 965–984. DOI: [10.1007/s00023-013-0262-8](#).

- [19] S. Carrozza and A. Tanasa. “ $O(N)$ Random Tensor Models”. In: *Letters in Mathematical Physics* 106.11 (Aug. 2016), pp. 1531–1559. DOI: [10.1007/s11005-016-0879-x](https://doi.org/10.1007/s11005-016-0879-x).
- [20] V. Bonzom, V. Nador, and A. Tanasa. “Double scaling limit for the $O(N)^3$ -invariant tensor model”. In: *Journal of Physics A: Mathematical and Theoretical* 55.13 (Mar. 2022), p. 135201. DOI: [10.1088/1751-8121/ac4898](https://doi.org/10.1088/1751-8121/ac4898).
- [21] V. Bonzom, V. Nador, and A. Tanasa. “Diagrammatics of the quartic $O(N)^3$ -invariant Sachdev-Ye-Kitaev-like tensor model”. In: *Journal of Mathematical Physics* 60 (July 2019), p. 072302. DOI: [10.1063/1.5095248](https://doi.org/10.1063/1.5095248).
- [22] S. Giombi et al. “Prismatic large N models for bosonic tensors”. In: *Physical Review D* 98.10 (Nov. 2018). DOI: [10.1103/physrevd.98.105005](https://doi.org/10.1103/physrevd.98.105005).
- [23] S. Prakash and R. Sinha. “Melonic dominance in subchromatic sextic tensor models”. In: *Physical Review D* 101.12 (June 2020). DOI: [10.1103/physrevd.101.126001](https://doi.org/10.1103/physrevd.101.126001).
- [24] G. Chapuy, M. Marcus, and G. Schaeffer. “A bijection for rooted maps on orientable surfaces”. In: (2007). DOI: [10.48550/ARXIV.0712.3649](https://doi.org/10.48550/ARXIV.0712.3649).
- [25] R. Gurau and G. Schaeffer. *Regular colored graphs of positive degree*. 2013. DOI: [10.48550/ARXIV.1307.5279](https://doi.org/10.48550/ARXIV.1307.5279).
- [26] R. Gurau, A. Tanasa, and D. R. Youmans. “The double scaling limit of the multi-orientable tensor model”. In: *EPL (Europhysics Letters)* 111.2 (July 2015), p. 21002. DOI: [10.1209/0295-5075/111/21002](https://doi.org/10.1209/0295-5075/111/21002).
- [27] L. Lionni and J. Thürigen. “Multi-critical behaviour of 4-dimensional tensor models up to order 6”. In: *Nuclear Physics B* 941 (Apr. 2019), pp. 600–635. DOI: [10.1016/j.nuclphysb.2019.02.026](https://doi.org/10.1016/j.nuclphysb.2019.02.026).
- [28] P. Di Francesco. “2D quantum gravity, matrix models and graph combinatorics”. In: *NATO Advanced Study Institute: Marie Curie Training Course: Applications of Random Matrices in Physics*. June 2004, pp. 33–88. arXiv: [math-ph/0406013](https://arxiv.org/abs/math-ph/0406013).
- [29] P. Di Francesco, P. H. Ginsparg, and J. Zinn-Justin. “2-D Gravity and random matrices”. In: *Phys. Rept.* 254 (1995), pp. 1–133. DOI: [10.1016/0370-1573\(94\)00084-G](https://doi.org/10.1016/0370-1573(94)00084-G). arXiv: [hep-th/9306153](https://arxiv.org/abs/hep-th/9306153).
- [30] L. Lionni and V. Rivasseau. *Intermediate Field Representation for Positive Matrix and Tensor Interactions*. 2016. DOI: [10.48550/ARXIV.1609.05018](https://doi.org/10.48550/ARXIV.1609.05018).
- [31] R. Kenyon. *An introduction to the dimer model*. 2003. DOI: [10.48550/ARXIV.MATH/0310326](https://doi.org/10.48550/ARXIV.MATH/0310326).
- [32] P. Flajolet and R. Sedgewick. *Analytic Combinatorics*. 1st ed. USA: Cambridge University Press, 2009. ISBN: 0521898064.

- [33] E. Fusy and A. Tanasa. “Asymptotic expansion of the multi-orientable random tensor model”. In: (2014). DOI: [10.48550/ARXIV.1408.5725](https://doi.org/10.48550/ARXIV.1408.5725).